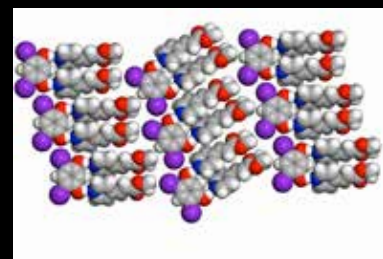
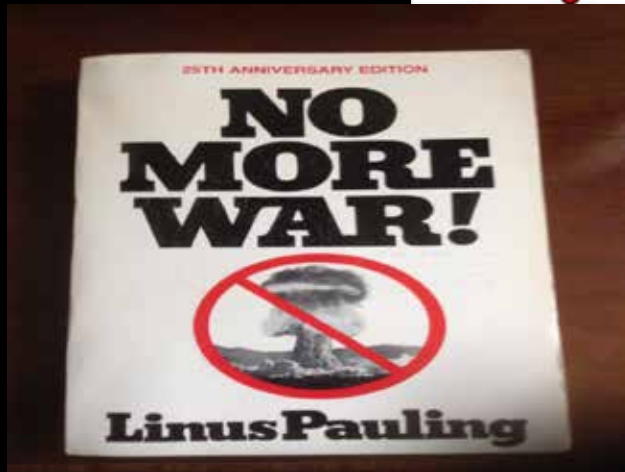
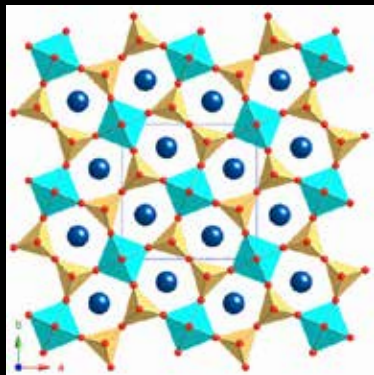
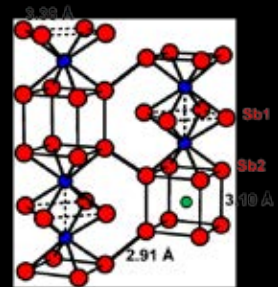
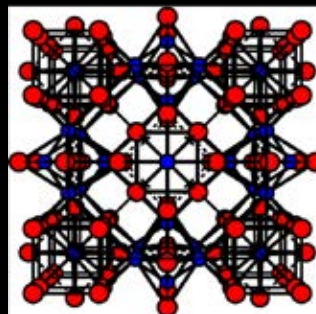
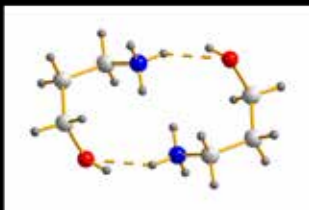
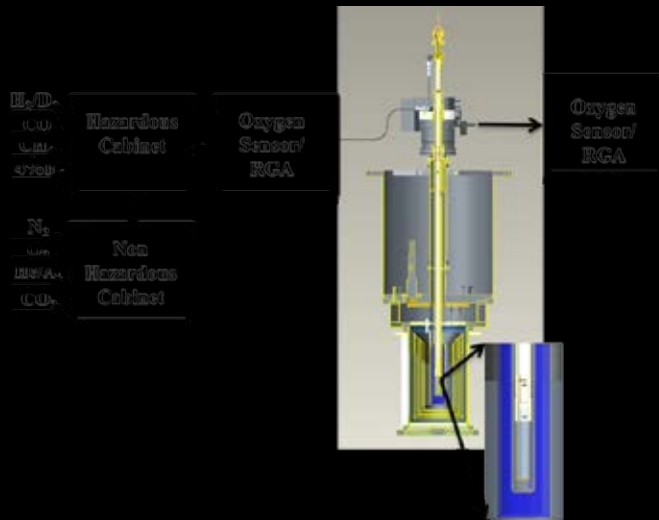
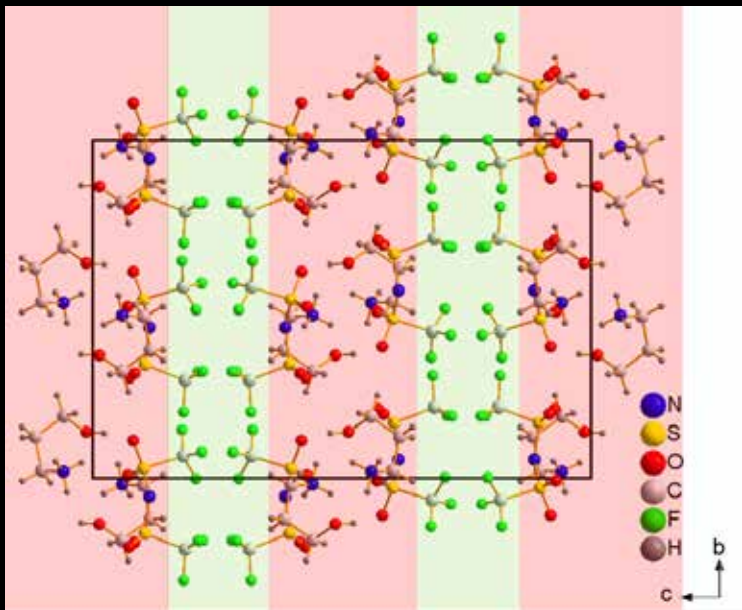


Crystallography for Sustainability



Transactions of the symposium held at the 2015 American Crystallographic Association Annual Meeting

Philadelphia, PA
July 25-29, 2015

Crystallography for Sustainability

Cora Lind-Kovacs, Robin Rogers, Organizers

Funding for this session provided, in part, by Crystal Growth & Design, Univ. of Toledo School of Green Chemistry & Engineering

Organic Synthesis in the Solid State Using Principles of Crystal Engineering Leonard R. MacGillivray	1
Crystallography and Sustainability John R. Helliwell	8
Two Step Reduction Process for the Synthesis of New Organic/Inorganic Hybrid Materials Containing Metals in Reduced Oxidation States Hans-Conrad zur Loye	20
Following the ‘Light Atoms’ in Energy Storage Devices Using Neutron Powder Diffraction Ashfia Huqq	31
Modifications of Mo_3Sb_7 via Chemical Substitution to Enhance the Thermoelectric Properties Holger Kleinke	38
Elucidating the Structure of Ionic Liquids by SXR, SAXS and WAXS New Opportunities for Materials Design	46
Anja V. Mudring	

PHOTOSTABLE CO-CRYSTALS OF (*E*)-METHYL-3-(PYRIDIN-4-YL)PROP-2-ENOATE INVOLVING ISOSTERIC RESORCINOLS: EFFECTS OF SECONDARY INTERACTIONS INVOLVING TEMPLATES

Elizabeth Elacqua, Ryan H. Groeneman, and Leonard R. MacGillivray*
Department of Chemistry, University of Iowa, Iowa City, IA 52242, USA

Eric W. Reinheimer
*Department of Chemistry and Biochemistry, W.M. Keck Foundation Center for
Molecular Structure, California State University San Marcos, San Marcos, CA 92096,
USA*

1. ABSTRACT

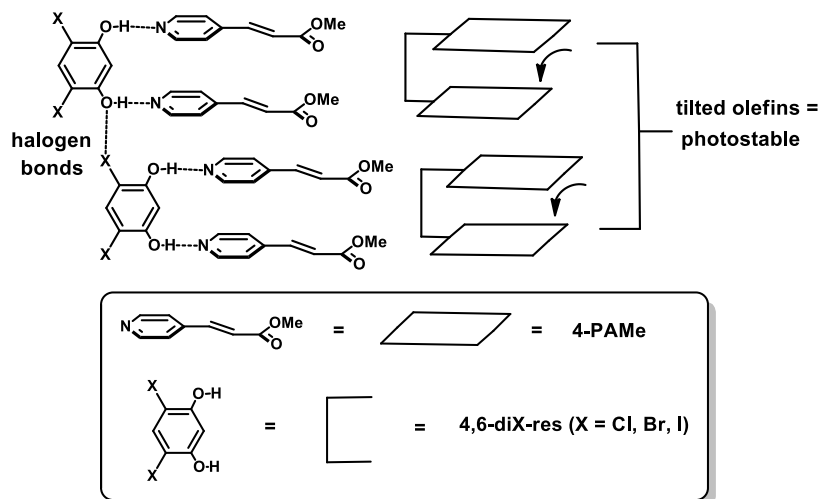
Three photostable co-crystals involving (*E*)-methyl-3-(pyridin-4-yl)prop-2-enoate and members of a series of isosteric resorcinols based on 4,6-di-X-res (where: X = Cl, Br, I; res = resorcinol) are described. In each case, a three-component hydrogen-bonded assembly was achieved that was determined to be photostable upon exposure to ultraviolet irradiation. Roles of secondary forces in the form of halogen bonding (*i.e.* X \cdots X and X \cdots O forces) and C-H \cdots O hydrogen bonds in contributing to the photostabilities are addressed.

2. INTRODUCTION

The organic solid state is an attractive medium to direct and control chemical reactivity. Products difficult to achieve in solution (*e.g.* ladderanes [1] and cyclophanes [2]) can be realized in solids. A solid-state reaction most often studied is the photoinduced [2+2] cycloaddition reaction, where two adjacent carbon-carbon double (C=C) bonds react to produce two C-C bonds in the form of a cyclobutane ring. In recent years, the [2+2] photodimerization has been controlled with significant degrees of success in solids using small organic molecules[3], as well as inorganic complexes [4], as ditopic templates. The templates assemble and align olefins within discrete supramolecular assemblies with structures that largely adhere to the strict geometry criteria of Schmidt for photoreaction in a solid [5].

In this context, we have demonstrated that ditopic molecules based on resorcinol (res) can reliably direct [2+2] photodimerizations in the solid state. The method relies on the ability of the 1,3-dihydroxy groups to assemble and enforce face-to-face stacking of olefins within discrete hydrogen-bonded assemblies. The discrete assemblies possess structures largely devoid of vexatious effects of long-range packing that can hinder olefins from adopting prerequisite geometry criteria to react [6]. With this in mind, we report here on structural origins related to long-range packing that govern the photostabilities of three co-crystals involving (*E*)-methyl-3-(pyridin-4-yl)prop-2-enoate (4-PAMe) as the reactant and three isosteric res based on 4,6-di-X-res (where: X = Cl, Br, I) as templates. We show that secondary interactions involving the

halogen atoms of the templates support the formation of stacked assemblies with olefins that adopt photostable geometries. The halogen bonds support the formation of columns wherein horizontal tilt angles place the stacked C=C bonds in a displaced geometry that renders the solids photostable. C-H...O hydrogen bonds involving 4-PAMe are also described to support the photostabilities.



Scheme 1

3. EXPERIMENTAL

3.1 Co-crystal Formations

4-PAMe was synthesized according to a modified procedure [7]. Co-crystals of (4,6-diCl-res)·2(4-PAMe), (4,6-diBr-res)·2(4-PAMe), and (4,6-diI-res)·2(4-PAMe) were prepared by dissolving 50 mg of 4-PAMe in 5 mL of ethanol. Each resulting solution was added to a 2 mL solution of 0.5 mol equivalents of each res in ethanol. Within periods of 1 to 3 d, colorless single crystals formed. The crystals were filtered, dried, and analyzed using single-crystal X-ray diffraction. All co-crystals were exposed to UV light from a 500 W medium-pressure Hg lamp within a photochemistry cabinet for approximately 150 h. The lack of photoreactivity of each co-crystal was indicated by the absence of a characteristic cyclobutane peak in the ¹H NMR spectra (Bruker Avance 400 MHz, DMSO-*d*₆ as solvent).

3.2 X-ray Crystallography

Single crystals of each co-crystal were secured to cryoloops using Dow Corning grease. Diffraction data were collected using a Rigaku SCXMini X-ray diffractometer equipped with a Rigaku Mercury 70 CCD camera. Data collection strategies to ensure maximum data redundancy were determined using CrystalClear [8]. Data collection, initial indexing, frame integration, Lorentz-polarization corrections and final cell parameter calculations were conducted using CrystalClear. Multi-scan absorption corrections were performed using REQAB. In all cases, the solutions included anisotropic temperature factors on all non-hydrogen atoms. All structural refinements were performed using SHELX-97 [9].

Table 1. Crystallographic parameters for (4,6-di-X-res)·2(4-PAMe).

Compound	(4,6-diCl-res)·2(4-PAMe)	(4,6-diBr-res)·2(4-PAMe)	(4,6-diI-res)·2(4-PAMe)
----------	--------------------------	--------------------------	-------------------------

CCDC code	963681	963680	963682
Formula	C ₂₄ H ₂₂ Cl ₂ N ₂ O ₆	C ₂₄ H ₂₂ Br ₂ N ₂ O ₆	C ₂₄ H ₂₂ I ₂ N ₂ O ₆
Formula weight	505.34	594.26	688.24
Temperature, K	293(2)	293(2)	293(2)
Space group	<i>P</i> $\bar{1}$	<i>P</i> $\bar{1}$	<i>C</i> 2/c
<i>a</i> , Å	7.3669(3)	9.0804(6)	20.9315(14)
<i>b</i> , Å	11.7964(5)	11.3687(8)	9.3442(6)
<i>c</i> , Å	14.9896(10)	13.1717(9)	27.0740(19)
α , deg	71.296(5)	85.632(6)	90.00
β , deg	85.657(6)	88.242(6)	95.619(7)
γ , deg	82.660(6)	67.785(5)	90.00
Volume, Å ³	1222.90(11)	1255.16(15)	5269.9(6)
<i>Z</i>	2	2	8
Density (calc), g/cm ³	1.372	1.572	1.735
μ , mm ⁻¹	0.307	3.270	2.426
Scan	ω scan	ω scan	ω scan
θ range, deg	3.09-27.48	2.99-25.34	3.02-25.35
Reflections measured	12806	11115	21471
Independent reflns.	5571	4562	4819
Independent reflns [<i>I</i> >2 σ]	4093	3391	3517
Data/restraints/param	5571/0/317	4562/0/317	4819/0/311
<i>R</i> _{int}	0.0195	0.0377	0.0369
Final <i>R</i> Indices [<i>I</i> >2 σ]	<i>R</i> ₁ = 0.0462, <i>wR</i> ₂ = 0.1146	<i>R</i> ₁ = 0.0420, <i>wR</i> ₂ = 0.0784	<i>R</i> ₁ = 0.0476, <i>wR</i> ₂ = 0.0939
<i>R</i> Indices (all data)	<i>R</i> ₁ = 0.0661, <i>wR</i> ₂ = 0.1267	<i>R</i> ₁ = 0.0653, <i>wR</i> ₂ = 0.0862	<i>R</i> ₁ = 0.0681, <i>wR</i> ₂ = 0.1020
Goodness-of-fit on <i>F</i> ²	1.043	1.064	1.063

$$R_1 = \frac{\sum ||F_o| - |F_c||}{\sum |F_o|}, \quad wR_2 = \frac{[\sum [w(F_o^2 - F_c^2)^2]}{\sum [w(F_o^2)^2]}^{1/2}$$

$$\text{Goodness-of-fit} = \frac{[\sum w(|F_o| - |F_c|)^2 / (N_{\text{obs}} - N_{\text{parameter}})]^{1/2}}$$

4. RESULTS AND DISCUSSION

We have reported on the solid-state reactivity of 4-PAMe in an organic protecting group strategy made possible *via* the solid state [10]. Co-crystallization of 4-PAMe with up to 10 different res derivatives as templates afforded co-crystals that were largely photostable. The photostabilities contrasted the high degree of reactivity of the stilbazole 4[2-(4-pyridinyl)ethenyl]methylbenzoate (4-PBAMe) involving the same res templates. To gain insight into the marked photostability of 4-PAMe, we have studied the solid-state assembly of 4-PAMe with members of the series 4,6-di-X-res (where: X = Cl, Br, I). We expected the isosteric relationship of the res, wherein the molecules differ only in pendant substitutions of isosteres [11], to lend to the formation of

similar crystal structures that, in turn, would allow us to gain an understanding into the origin of the photostabilities.

Single-crystal X-ray analyses of (4,6-di-X-res)·2(4-PAMe) (where: X = Cl, Br, or I) revealed the formation of discrete, three-component hydrogen-bonded assemblies in each solid. For X = Cl and Br, the components crystallize in the triclinic space group $P\bar{1}$, while for X = I the components crystallize in the monoclinic space group $C2/c$. In each case, the molecules of 4-PAMe are sustained by two O-H···N hydrogen bonds wherein two olefins are juxtaposed adjacent to each res in a face-to-face π -stacked geometry (Figure 1, Table 2). The stacked pyridine rings of 4-PAMe are tilted out of the plane of each res, as demonstrated by pyr···res tilt angles that range from 42.4 to 64.7° (Table 2). For comparison, structural data for the reported photoactive co-crystal (5-F-res)·2(4-PAMe) are given [10]. The C=C bonds within each hydrogen-bonded assembly are separated by 4.02 Å, 4.22 Å, and 4.31 Å for X = Cl, Br, and I, respectively. The separation distances generally lie at the upper limit (X = Cl) and beyond (X = Br, I) the distance criterion of Schmidt for a [2+2] photodimerization in a solid.

Table 2. Olefin metrics within discrete hydrogen-bonded assemblies based on (4-PAMe).

X-res	O···N (Å)	pyr···res tilt (°)	C=C separation (Å)	D ₁ (Å)	D ₂ (Å)
4,6-diCl	2.721(2) 2.781(2)	64.6, 64.7	4.02	0.70	1.34
4,6-diBr	2.710(5) 2.766(5)	50.2, 55.9	4.22	0.31	2.25
4,6-diI	2.705(7) 2.765(8)	42.4, 55.0	4.31	0.37	2.23
5-F ¹⁰	2.741(2) 2.763(2)	85.1, 87.1	3.73	0.78	0.92

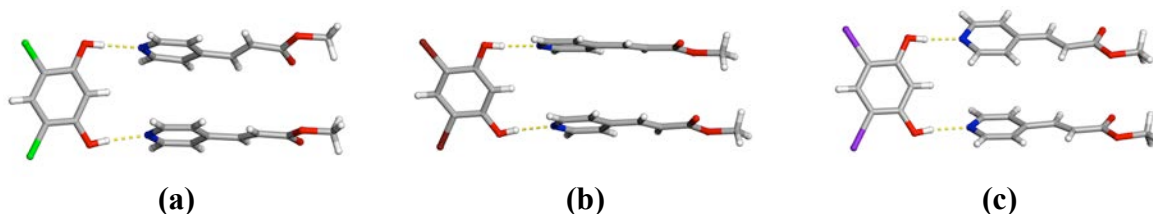


Figure 1. X-ray crystal structures of (4,6-di-X-res)·2(4-PAMe) showing discrete, three-component assemblies: (a) X = Cl, (b) X = Br, (c) X = I.

A further examination of the stacked C=C bonds reveals that the olefins within each hydrogen-bonded assembly of (4,6-di-X-res)·2(4-PAMe) (where: X = Cl, Br, or I) lie offset. Ramamurthy has reported parameters that describe the geometry of two stacked C=C bonds that lie in close proximity to undergo reaction in a solid [12]. Of interest, for (4,6-di-X-res)·2(4-PAMe), are D₁ and D₂ parameters, which correspond to lateral displacements along the axis of 4-PAMe and approximately normal to the plane of each res ring, respectively (Table 2) [13]. For (4,6-di-X-res)·2(4-PAMe), the pairs of stacked C=C bonds in each hydrogen-bonded assembly exhibit appreciably large D₂ or lateral displacements normal to the plane of each res. Specifically, the

D_2 values range from 1.34 to 2.25 Å for photostable (4,6-di-X-res)·2(4-PAMe) (Figure 2), with D_2 for photoactive (5-F-res)·2(4-PAMe) being 0.92 Å.

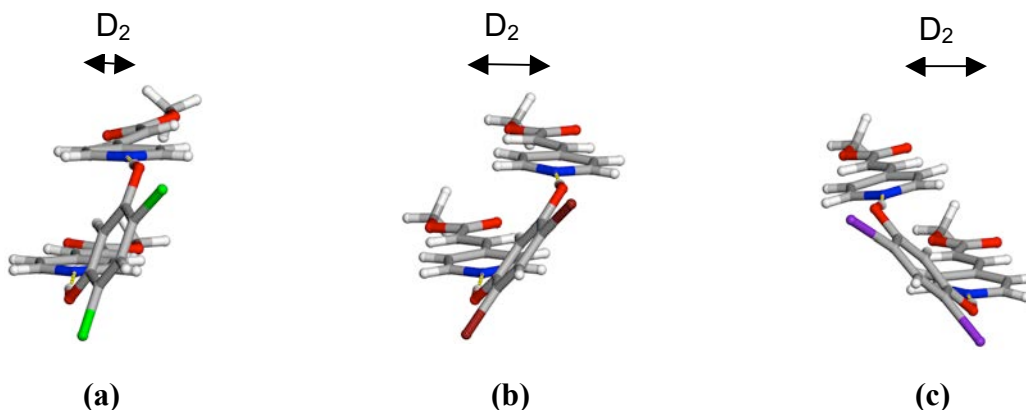


Figure 2. X-ray structures of (4,6-di-X-res)·2(4-PAMe) highlighting D_2 (lateral displacement normal to res ring: (a) X = Cl, (b) X = Br, and (c) X = I.

That the stacked C=C bonds in (4,6-di-X-res)·2(4-PAMe) (where: X = Cl, Br, or I) exhibit large D_2 values can be attributed to secondary interactions involving the halogen atoms of the *ortho*-disubstituted templates. In particular, the assemblies pack to form either a quadruple (X = Cl) or linear stacked arrays (X = Br, I). For X = Cl, the assemblies stack anti-parallel to give localized quadruple stacks sustained by Type I Cl···Cl interactions (Cl···Cl = 3.445(1) Å) (Figure 3a) [14]. The quadruple stacks lie offset to form a 2D layered structure that is canted to the crystallographic *bc*-plane. For X = Br and I, the assemblies form infinite 1D columns sustained by Type II O···X forces (O···Br 3.247(3), O···I 3.401(4) Å) (Figures 3b,c). Similar to (4,6-di-Cl-res)·2(4-PAMe), the columns form a 2D layered structure perpendicular to the *bc*-plane. The C=C separations between nearest-neighbor assemblies, with exception to X = Cl (separation: 3.94 Å), are beyond the limit of Schmidt for photodimerization [separation (Å): 5.48 (Br), 5.54 (I)][15]. Collectively, the interactions involving the halogen atoms effectively act to constrain each res molecule within a 2D plane. The tilted and offset stackings of 4-PAMe can, thus, be attributed to structure demands of dense packing wherein each 4-PAMe undergoes a tilt to optimize both face-to-face stacking and packing (Figure 3d) [16]. Each olefin also participates in a dimeric array of C-H···O hydrogen bonds (C···O (Å): 3.344(3), 3.346(3), 3.437(3), and 3.528(3) for Cl, 3.331(4), 3.354(6), 3.431(4), and 3.468(5) for Br, 3.297(10), 3.338(9), 3.356(10), and 3.416(10) for I), which may suppress molecular movements that favor a reaction (Figure 3e) [12].

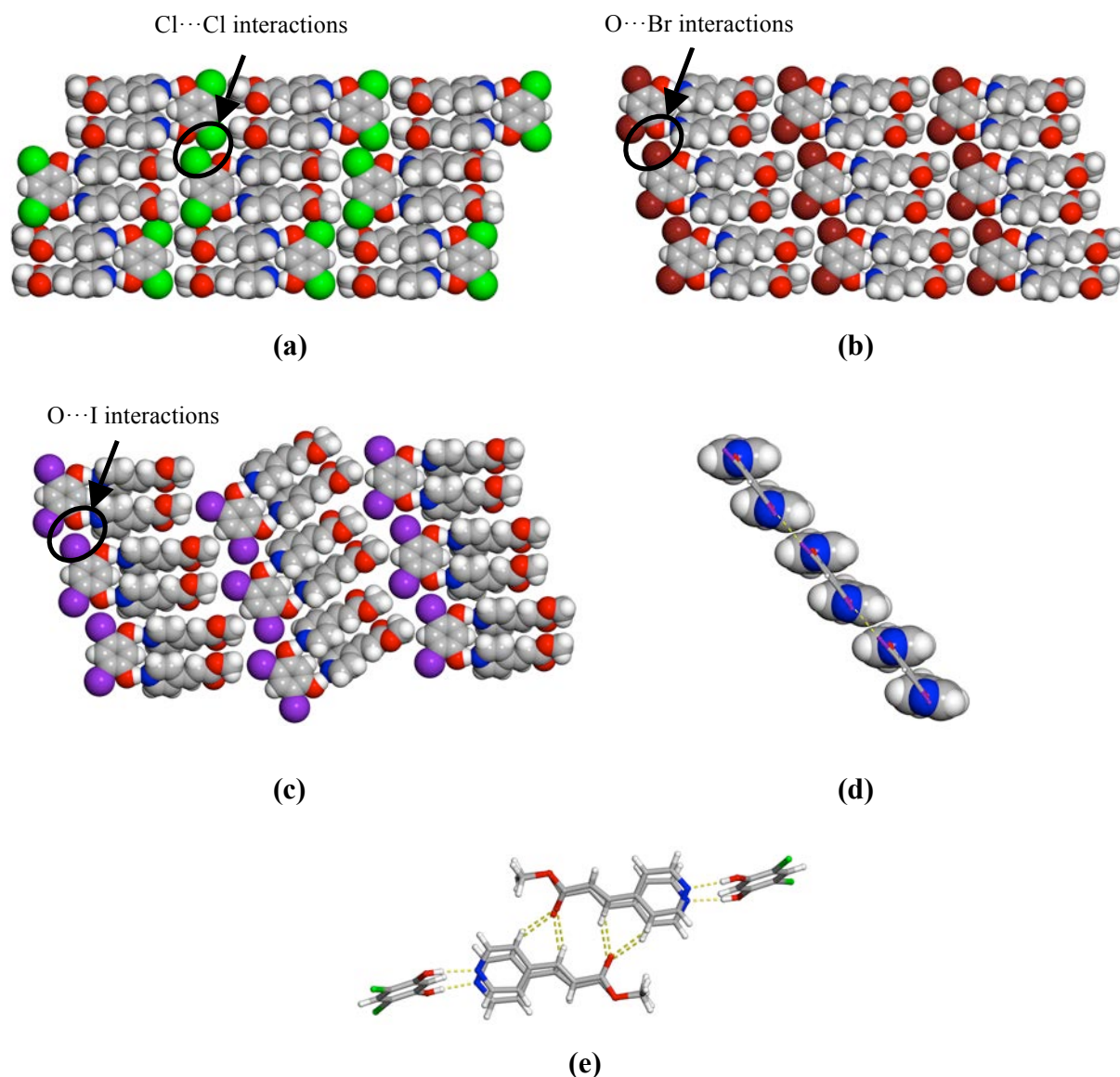


Figure 3. Extended 2D packings of (4,6-di-X-res)·2(4-PAMe): (a) Cl···Cl interactions, (b) O···Br interactions, (c) O···I interactions, (d) side view of tilt angle (X = I), and (e) C-H···O hydrogen bonds (X = Cl).

5. CONCLUSION

In this contribution, we have described three photostable co-crystals based on a series of res in (4,6-di-X-res)·2(4-PAMe). Origins of the photostabilities have been ascribed to secondary interactions involving halogen atoms on the res templates, which support tilted stacking and packing of the olefins. We are now studying related co-crystals involving 4-PAMe to determine additional factors that affect reactivities in organic solids.

6. ACKNOWLEDGEMENTS

We are grateful to the National Science Foundation (L.R.M., DMR-1408834) for funding. The authors would also like to acknowledge California State University San Marcos for the funds to purchase the Rigaku SCXMini X-ray diffractometer.

7. REFERENCES

- [1] X. Gao, T. Frišćić, and L. R. MacGillivray, *Angew. Chem. Int. Ed.* 43 (2004), 232.
- [2] (a) T. Frišćić and L. R. MacGillivray, *Chem. Commun.* (2003), 1306; (b) E. Elacqua, T. Frišćić, and L. R. MacGillivray, *Isr. J. Chem.* 52 (2012), 53.
- [3] (a) L. R. MacGillivray, G. S. Papaefstathiou, T. Frišćić, T. Hamilton, D.-K. Bučar, Q. Chu, D. B. Varshney, and I. G. Georgiev, *Acc. Chem. Res.* 41 (2008), 280; (b) B. R. Bhogala, B. Captain, A. Parasarthy, and V. J. Ramamurthy, *J. Am. Chem. Soc.* 132 (2010), 13434.
- [4] (a) G. S. Papaefstathiou, Z. Zhong, L. Geng, and L. R. MacGillivray, *J. Am. Chem. Soc.* 126 (2004), 9158; (b) M. Nagarathinam, A. M. P. Peedikakkal, and J. J. Vittal, *Chem. Commun.* (2008), 5277; (c) I. G. Georgiev, D.-K. Bučar, and L. R. MacGillivray, *L. R. Chem. Commun.* (2010), 4956.
- [5] G. M. J. Schmidt, *Pure Appl. Chem.* 27 (1971), 647.
- [6] L. R. MacGillivray, *J. Org. Chem.* 73 (2008), 3311.
- [7] K. C. Agarwal and E. E. Knaus, *J. Heterocyclic Chem.* 22 (1985), 65.
- [8] J. W. Pflugrath, *Acta Crystallogr. D* 55 (1999), 1718.
- [9] G. M. Sheldrick, *SHELXL, Program for the Crystal Structure Refinement*; University of Göttingen: Göttingen, 1997.
- [10] E. Elacqua, P. Kaushik, R. H. Groeneman, J. C. Sumrak, D.-K. Bučar, and L. R. MacGillivray, *Angew. Chem. Int. Ed.* 51 (2012), 1037.
- [11] A. G. Dikundwar, U. D. Pete, C. M. Zade, R. S. Bendre, and T. N. G. Row, *Cryst. Growth Des.* 12 (2012), 4530.
- [12] V. Ramamurthy and K. Venkatesan, *Chem. Rev.* 87 (1987), 433.
- [13] Parameters defined: D_1 = displacement of the double bonds along the molecular axis, D_2 = perpendicular displacement of the double bonds along the molecular axis (see ref. 12).
- [14] A. Mukherjee, S. Tothadi and G. R. Desiraju, *Acc. Chem. Res.* 47 (2014), 2514.
- [15] The D_2 displacement for X = Cl (1.34 Å) is in line with the photostability of the solid.
- [16] R. Taylor, *CrystEngComm.* 16 (2014), 6852.

CRYSTALLOGRAPHY AND SUSTAINABILITY

John R. Helliwell

School of Chemistry, University of Manchester, Brunswick Street, Manchester M13 9PL, UK

Crystallography has played several major roles in sustainability including, on the science side (*e.g.* new drug discovery and new materials for energy usage) and in education initiatives (*e.g.*, most recently within the IYCr). On the social side as a field we have done much towards the empowerment of women, including three female IUCr Presidents, and towards World Peace. The preservation of our processed diffraction and derived molecular coordinate data via our databases and linking to publications is also highly notable within our discipline. IUCr has helped facilitate the now universally harnessed crystallographic information file ‘cif’, led the way with the linking of publications to diffraction and atomic coordinate data in the IUCr journals and most recently is assisting in the debate about and developing tools for preservation of raw diffraction data. A major part of the sustainable industrial future involves nanomaterials not least using smaller quantities of materials. The IUCr is taking an active role in a CODATA/VAMAS Joint Working Group on the Description of Nanomaterials to help develop a uniform description system for nanomaterials as an essential step towards reproducibility of their production. Another major feature of crystallography in the life sciences is the use of synchrotron radiation in macromolecular structure determination including its applications in the pharmaceutical industry.

1. INTRODUCTION

Firstly what is ‘sustainability’? Wikipedia provides I think a readily available and helpful description [1]:-

*“The world's sustainable development goals are integrated into the eight **Millennium Development Goals (MDGs)** that were established in 2000 following the Millennium Summit of the United Nations. Adopted by the 189 United Nations member states at the time and more than twenty international organizations, these goals were advanced to help achieve the following sustainable development standards by 2015:*

- 1. To eradicate extreme poverty and hunger*
- 2. To achieve universal primary education*
- 3. To promote gender equality and empower women*
- 4. To reduce child mortality*
- 5. To improve maternal health*
- 6. To combat HIV/AIDS, malaria, and other diseases*
- 7. To ensure environmental sustainability*
- 8. To develop a global partnership for development”*

Crystallography most obviously is assisting with goal 6. Furthermore crystallography has, since its earliest period when William Henry Bragg had a substantial fraction of his research students being female, had an excellent proportion of its researchers being female. In our field gender

equality at the ‘breaking the glass ceiling level’ has occurred. We have seen three female IUCr Presidents namely Kathleen Lonsdale, Dorothy Hodgkin and Sine Larsen (1966^{*}, 1981 to 1984 and 2008 to 2011). There are also female crystallographers up to Nobel Prize winner level with Dorothy Hodgkin (Nobel Prize in Chemistry 1964) and Ada Yonath (Nobel Prize in Chemistry, shared, 2009). Crystallography research therefore has assisted in goal 3. I have endeavoured to assist in this process albeit in a small way via my work as Gender Equality Champion at the School of Chemistry in the University of Manchester (see section 3) via the Athena SWAN framework of the UK Government’s Equality Challenge Unit [2].

Goal 2: Assisting the realisation of the goal ‘*To achieve universal primary education*’, is less easy perhaps as crystallography is in its details built around the core sciences and mathematics, rather beyond what I understand as ‘primary education’, which refers to early school years. ‘Primary education’ presumably means ‘reading, writing and arithmetic’ basic skills. If we diversify this goal then we can say that we have numerous ways of reaching out to school children, as well as the Public.

As a probably extreme example, when I started my enquiries about giving a lecture on crystallography in prisons I was alerted to the quite often low education skills I might expect in my audience. As I have yet not managed to give a lecture to this audience my practical knowledge of how to proceed is at the embryonic stage. My ideas include to especially take advantage of the highly visual materials that one has available such as crystals (calcite, quartz, and so on) and molecular models. There is in fact precedent: “*Bringing science & nature into prisons and so inspire*” [4]; it can be done.

Very importantly, within the IUCr’s IYCr, much of the effort of IYCr was directed toward outreach and universal education, including a launch video describing the relevance of crystallography to many aspects of sustainable scientific and technological development (subtitled in 28 world languages) [5], a 20-page booklet describing the role of crystallography in the modern world (in 16 different languages) [6] and a selection of IYCr activities directed at schoolchildren [7].

Regarding Goal 8 I think we can reasonably say that the International Union of Crystallography itself, through community participation in IUCr of all the recognised crystallographic associations, national and regional, in the World does contribute in a major way with the aim “To develop a global partnership for development”. Indeed IUCr’s membership and active participation in the International Council for Science (ICSU [8]), CODATA (ICSU’s Committee on Data for Science and Technology [9]) and the International Council for Scientific and Technical Information (ICSTI [10]) and other international organisations affirms further its active contributions to Goal 8. I represented IUCr for 9 years at ICSTI and have commenced my first formal term of office representing IUCr at CODATA (from 2014).

* Just before the Seventh General Assembly in 1966, the then President, J.D. Bernal, resigned for reasons of health. In accordance with By-Law 2.3 (version after amendment by the Sixth General Assembly), Dame Kathleen Lonsdale assumed the office of President until the close of the Seventh General Assembly [3].

For a current overview perspective of such global challenges facing the sciences, and the social sciences, I commend to you the lecture to the American Association for the Advancement of Science (AAAS) of Dr. Heide Hackmann, Executive Director of ICSU and who holds a PhD in science and technology studies from the University of Twente in the Netherlands [11].

2. CRYSTALLOGRAPHY RESEARCH EXAMPLES RELEVANT TO SOCIETY

2.1 Research

Crystallography's role in improving health and efficient energy usage are already, and can be increasingly so, at the molecular level based on crystal structure analyses. In health sciences, structure-based drug design is routinely employed; in energy research hydrogen storage is addressed also using 3D atomic structures. Thus crystallography has an important role within the topic of the sustainability of Life. These particular topics are covered in detail by others in this ACA Transactions Symposium.

2.2 Knowledge transfer

In terms of Knowledge Transfer in research, as an example, I cite that the Research Councils UK undertook an analysis, and indeed highly commended the wider impacts, of the UK's Synchrotron Radiation Source (SRS) protein crystallography effort, which spanned the operational period 1981 to 2008, based at Daresbury Laboratory [12]. To meet the needs of commercial customers, Daresbury Laboratory established DARTS (Daresbury Analytical Research and Technology Service) especially based around the SRS instruments for protein crystallography [13], chemical crystallography and powder diffraction, with research impact case studies and research publications surveys).

2.3 Nanomaterials and our role as crystallographers to help properly characterise them

A Joint Working Group on the Description of Nanomaterials has been set up by CODATA/VAMAS [14] and from which I quote:-

“Nanomaterials are complex, and researchers continue to develop new and innovative materials. Describing nanomaterials is a challenge for all user communities, but a description system is essential to ensure that everyone knows exactly which nanomaterial is being discussed, whether for research, regulatory, commercial, or other purposes.

CODATA and VAMAS, an international pre-standardization organization concerned with materials test methods, have set up a joint working group to help develop a uniform description system for nanomaterials. This international working group includes representatives from virtually every scientific and technical discipline involved in the development and use of nanomaterials, including physics, chemistry, materials science, pharmacology, toxicology, medicine, ecology, environmental science, nutrition, food science, crystallography, engineering, and more. Many international scientific unions actively participate.”

The IUCr is one of these active participants. Nanomaterials are one of the most actively pursued areas of modern day materials research, and can be expected to considerably assist with reducing the quantities of materials used in products and appliances, which is an identified pre requisite for example in helping with the sustainability of use of rare chemicals.

2.4 Overarching data policy and the principle of open access

The IUCr took part in the Working Group of ICSU that produced a widely regarded Report on Open Access [15] and which emphasised the following goals:-

“The International Council for Science advocates the following goals for open access. The scientific record should be:

- *free of financial barriers for any researcher to contribute to;*
- *free of financial barriers for any user to access immediately on publication;*
- *made available without restriction on reuse for any purpose, subject to proper attribution;*
- *quality-assured and published in a timely manner; and*
- *archived and made available in perpetuity.*

These goals apply both to peer-reviewed research publications, the data on which the results and conclusions of this research are based, and any software or code used in the course of the research.”

Furthermore in the World of research the ICSU report correctly stated that:-

“The process of scientific discovery involves researchers being able to communicate their research results and audiences being able to access these results. At the same time, not all researchers have ready access to research funding and cost must not be a barrier to placing their results in the most appropriate journal, data repository or other outlet for that research.”

It can be estimated that **funded research** comprises a minority of the research that is undertaken. IUCr is a global international union of crystallographers and spans countries that are often termed:- the developed world, the developing world and the poorest nations. Therefore finding sustainable ways to link scientific publications to data is a paramount concern and also to both maximise the science that is communicated by authors and to maximise the science that is accessed by readers.

Overall, in terms of data policy and open access, IUCr offers the fully funded and the unfunded researcher, whether early career or mature career, whether from the developed world or the developing world, free for author options and free for reader options. Thus crystallographic science is brought to the widest possible, global, range of research communities for the good of science and for society at large.

2.5 Databases

A key part of this process of broad applicability rests on world wide access to the three dimensional (3D) structures database of biological macromolecules (Protein Data Bank) and the chemical crystallography databases (CCDC, ICDD, COD, Metals). These provide fantastic resources spanning a vast range of the living and material world in atomic detail. The tools of physics (X-rays, neutrons and electrons in diffraction, microscopies and spectroscopies) allow us to determine and study in detail these structures and their atomic interactions and increasingly to study their structural dynamics [16]. Clear technical understanding of these physical methods provides clarity on how much trust we can place in the correctness of these structures ie their precision and accuracy. That said Professor Durward Cruickshank FRS (1924-2007) [17], my

esteemed crystallography research collaborator over several decades, was very concerned about the lack of a coordinate error on an atom in a PDB file. He launched the diffraction precision index [18] as an average error on a finalised refined protein crystal structure. I have extended that to estimating the error on individual atoms and in association with colleagues in Bangalore made this into user accessible web tools [19,20].

Crystallography has a long tradition in community methods development, and in sharing derived and processed data at the databases referred to above. Research journals in this field have long provided links to derived data sets (molecular structures), and in more recent years to processed experimental data (single crystal X-ray structure factors and powder diffraction profiles); and in turn there have been links from curated data sets in structural databases back to the associated publication.

In crystallography as a whole and IUCr Journals in particular there are *stringent requirements* that articles will only be published with the accompanying data. Thus, in the life sciences, Protein Data Bank deposition files (derived coordinates and processed structure factor amplitudes) are obligatory to accompany a publication. At the submission stage of an article, information should be provided to convince the referees that the interpretations of the diffraction data and electron-density maps and/or structures are correct, within the resolution of the analysis; in the life sciences a Protein Data Bank structure validation report is what is currently required on submission. In chemical crystallography a submitted article must be accompanied by the ‘cif’ (the crystallographic information file) and includes atomic coordinates and structure factor amplitudes data; chemical crystallography is therefore the best exemplar of good practice as these are available to the handling editor and the referees to fully assess a crystallographic research article submission. An example can be found in [21].

Dataset requirement *recommendations* exist for articles that present experimental small-angle X-ray or neutron scattering data. For these, the deposition of an ASCII file representing the background-corrected scattering profile(s) with errors is recommended. For powder diffraction, articles that present the results of powder diffraction profile fitting or refinement (Rietveld) methods require deposition of the primary diffraction data, *i.e.* the numerical intensity of each measured point on the profile as a function of scattering angle.

Overall, the crystallographic databases provide the bed rock on which our publications rest. They allow readers to repeat any calculation that they wish in addition to reading the words in a publication. This is all a necessary pre requisite to contributing to a sustainable future based accurately and precisely on a full scientific record including data and information.

2.5.1 Extension to archiving of raw diffraction data: the IUCr Diffraction Data Deposition Working Group (IUCr DDDWG)

The latest discussions within IUCr are now looking towards archiving of raw diffraction data; the IUCr DDDWG’s inaugural triennial report for 2011 to 2014 can be found at the IUCr Forum devoted to the topic [22] and which also includes many relevant documents and inputs to a Public ie community wide discussion. *The Australian synchrotron data archive “Store.Synchrotron” is a best exemplar, whose work includes its support of users with publications having raw data sets, and its ability to manage DOI registration. This archive also*

releases raw diffraction image data sets for public analysis. For examples see references 23-29. In the USA the NIH has recently funded initiatives involving big data [30].

Universities in the UK in general and my own university in particular are, I know, also making great efforts in assisting its researchers with archiving of, and making available, raw data. As an example, of *due diligence towards Sustainability Goals involving improving human health*, I cite our research programme involving the platin anti-cancer agents binding to the amino acid histidine in a protein. We have made available numerous crystallographic diffraction images raw data sets as well as the processed diffraction amplitudes and the various derived coordinate data sets at the PDB [23]; these raw diffraction data sets have been placed firstly at the University of Utrecht [23] and promptly mirrored at the Australian data store [29] and then at the University of Manchester eScholar repository [31]. This timeline of stages arose because, although the X-ray diffraction data were measured in my Laboratory at the University of Manchester, the University, a pioneer with its data store, was not ready to host our raw data at the time of our publications. We were pioneers of making raw data available, within our university at least.

The descriptions in this section show the rigorous efforts made by crystallographers for several decades to archive their results along with the metadata being provided, to describe their data thoroughly as well as, now, extending where possible to making available the raw diffraction data sets.

3. CRYSTALLOGRAPHY AND GENDER EQUALITY

It is a major issue that women experience widespread inequality in making their way in science as a career. A perhaps less highlighted fact is that the natural talent, male and female, that we train to a very high standard as graduates in chemistry and physics and so on, respectively around 40% and 20 %, leads to around 5% being professors. The whole-of-UK University picture for Chemistry staff is presented in Figure 1. This is a massive discrepancy. We have to understand each stage of the academic career progression path and do much better at assisting women at each of these career development hurdles. Otherwise we will continue to see this huge loss of trained scientific talent. In the UK we have a scheme called Athena SWAN, a marvellous initiative of our UK Government [2], and I am glad to have played a role in trying to help [32].

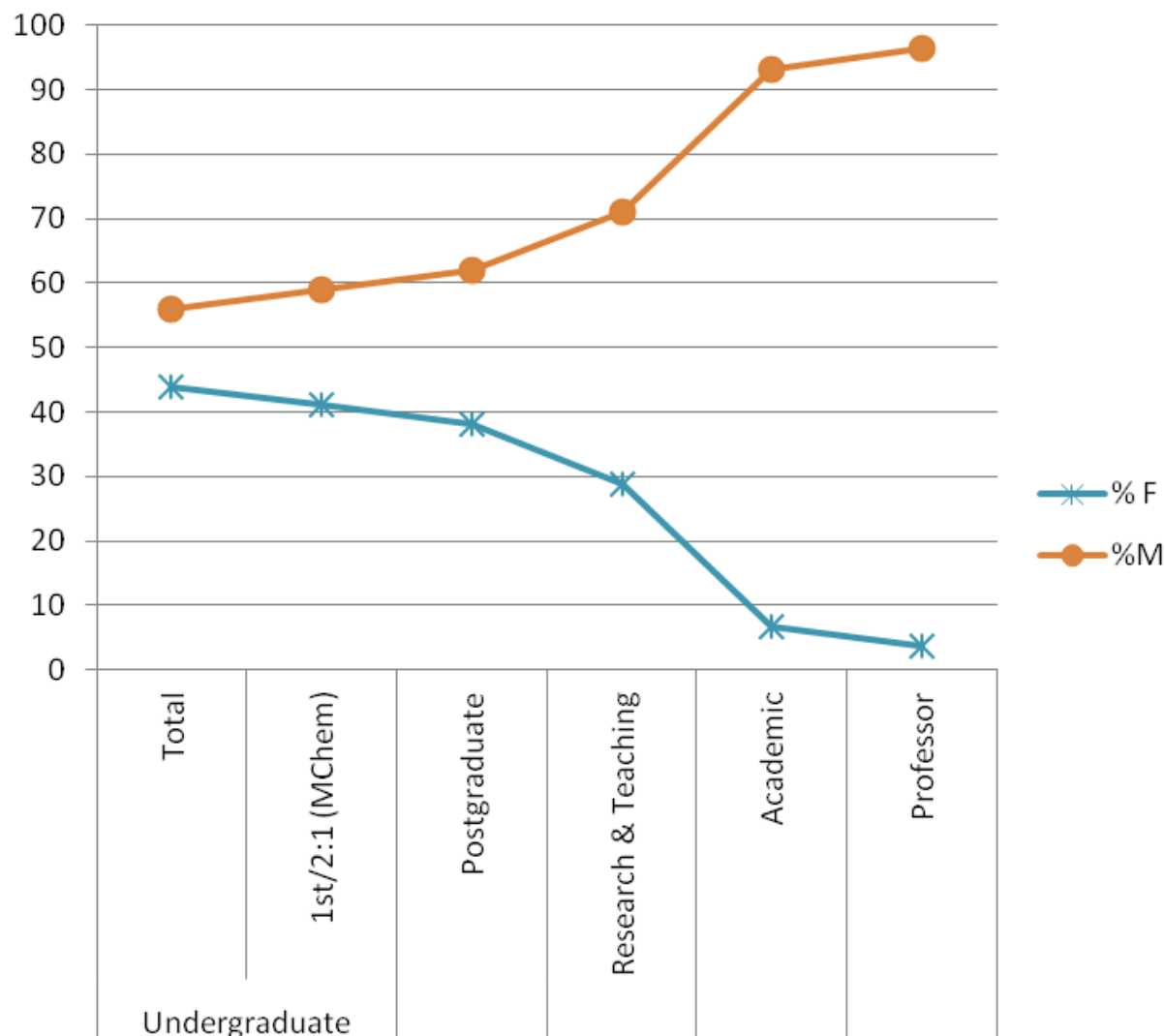


Figure 1. Progression of females in Chemistry in the UK for a year (data shown are for 2011/12 but are typical). The situation for Physics in the UK is very similar with female fractions at undergraduate (22%), postgraduate (26%), researcher 17%, lecturer (20%), senior lecturer (11%) and professor (5%).

4. CRYSTALLOGRAPHERS AND PEACE

It is striking to me that crystallographers have taken a prominent role trying to ensure Peace. There is surely a crucial role for sustainability of preserving peace!!

Professor Kathleen Lonsdale FRS, one of the two very first women to be elected to The Royal Society (in 1945), wrote a slim but powerfully argued book entitled “Is peace possible?” [33]; Figure 2. She went to jail during the Second World War for her beliefs as a pacifist.

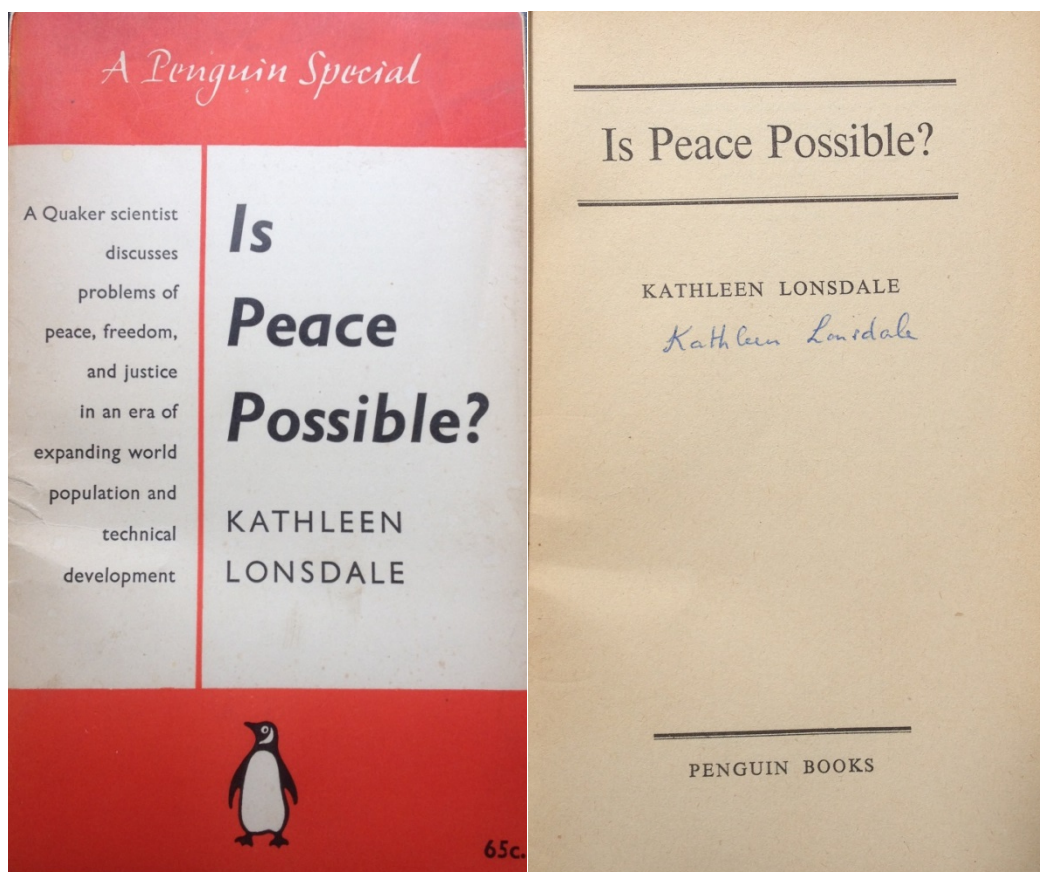


Figure 2. My own copy of Kathleen Lonsdale’s powerfully argued book entitled “Is peace possible?” [33]. I bought this copy from Amazon books and was very happy when I saw what truly looks to me to be the author’s signature!

Professor Dorothy Hodgkin FRS OM was President of Pugwash from 1976 to 1988. The Pugwash Conferences on Science and World Affairs bring together scholars and public figures to work towards reducing the danger of armed conflict and to seek solutions to global security threats [34]. In their “*Dialogue Across Divides*” Pugwash states:-

“We have to learn to think in a new way. Pugwash seeks a world free of nuclear weapons and other weapons of mass destruction. We create opportunities for dialogue on the steps needed to achieve that end, focusing on areas where nuclear risks are present. Moving beyond rhetoric, we foster creative discussions on ways to increase the security of all sides in the affected regions. Remember your humanity, and forget the rest.”

Professor Linus Pauling won two Nobel Prizes, one for chemistry (1954) and one for Peace (1962). Linus Pauling was obviously a great early practitioner of X-ray crystal structure analysis with a wide variety of his crystal structures featuring in his famous textbook on chemistry “The Nature of the Chemical Bond” [35]. He also wrote “No more War” (1958) [36] (Figure 3) and specifically his concerns about the safety level limits set for radiation:-

“I believe that the nations of the world that are carrying out the tests of nuclear weapons are sacrificing the lives of hundreds of thousands of people now living and of hundreds of thousands of unborn children, and that this sacrifice is unnecessary.”



Figure 3. My own copy of Linus Pauling’s “No more War” (1958) [36].

“Man has the intelligence to understand the universe, to appreciate the astounding complexity of the universe...Now man’s intelligence has provided him with the power to destroy himself, to bring an end to civilisation, an end to the human race. I believe that our intelligence, our common sense, is good enough to prevent this ultimate insanity.” Pages 14-15.

As Shakespeare wrote in Hamlet [37] sustaining Peace in the World has no easy answers:-

*“To be, or not to be? That is the question—
Whether ’tis nobler in the mind to suffer
The slings and arrows of outrageous fortune,
Or to take arms against a sea of troubles,
And, by opposing, end them?”*

Another of our IUCr Past Presidents, Sir Lawrence Bragg, when a young man, completed the First World War with distinguished military service as Major Lawrence Bragg OBE MC with great sound ranging achievements [38]. His and his Team's efforts basically reducing the length of the First World War considerably.

Where do we go from here as Crystallographers in terms of Planet Earth and Humanity? We can build on the work of Lawrence Bragg, Kathleen Lonsdale, Dorothy Hodgkin and Linus Pauling and many, many others of a sufficiently peaceful World to undertake basic and applied/sustainable research. The IYCr itself has created much new, important and good, interest in our field.

5. CONCLUSIONS AND WHERE WE MIGHT GO FROM HERE AS A CRYSTALLOGRAPHY RESEARCH COMMUNITY

In terms of data, one theme of this short article, we can reflect on the possible size of the crystallography data bases. If we assume a doubling period for data set entries of 10 years then in a 100 years from now a theoretical 2^{10} multiplication of entries would promise, if realized, an obviously amazing increase. In terms of database contents, given the myriad number of molecules, large and small, there apparently will be no limit to the number of new crystal structures. There will only be a limit set by our ingenuity of crystal structure determination. The role of crystallography in providing the clarity of 3D structure and thereby function will be a firm role in basic and applied science and thereby assisting with the sustainability of Life on Earth.

Our efforts to keep under active review, and to develop protocols for, the preservation of raw diffraction data are necessary and laudable, akin to the efforts made by astronomers and particle physicists, as due diligence for the research that we undertake and the data on which it firmly rests. As we have so many, and anticipate many more crystal structures, we may need to be selective about which raw diffraction data sets to preserve. Those research studies that can contribute to Public Health, improved energy sources and so on, vital for sustainability, can provide a useful criterion of where we should definitely preserve the raw diffraction data.

In terms of gender equality we have much in crystallography to be proud about but a great deal remains to be done. Indeed an improved retention of women in science through all the career stages is its own sustainability challenge (ie sustaining the development of trained talent in the field) and, through ICSU, IUCr can influence the whole of science significantly.

With IUCr Journals crystallography as a field is actually leading the development of the specific area of sustainability concerned with information and its links to data (including supporting data archiving wherever possible). Thus research effort is not lost, whilst making it available to other scientists as openly as possible within our capacities to do so. This in turn trains the widest range of talented professionals.

In terms of World Peace I imagine that the work in this area of Kathleen Lonsdale, Linus Pauling and Dorothy Hodgkin have contributed in a positive way to avoiding a nuclear conflict. On this, and obviously the work of many others to sustain a peaceful World, we can all build. Getting

nations to collaborate can be a major challenge. Our field, like particle physics and astronomy, has fine examples of collaboration that are international. The ones I have taken part in most actively are the European Synchrotron Radiation Facility (ESRF) in Grenoble, the Institut Laue Langevin in Grenoble and the European Spallation Source in Lund. The Middle East synchrotron radiation project ‘SESAME’ (Synchrotron-light for Experimental Science and Applications in the Middle East), is based in Jordan and whose history is described [39], is an important example of international collaboration and of capacity building. The genesis of the African Light Source project will be discussed in November 2015 at ESRF in Grenoble [40] set to be another fine example of capacity building if ways can be found to move it forward, which surely must be found. Crystallography as a field plays a very significant role in the synchrotron radiation, and neutron, facilities. These facilities have greatly expanded our scope, in many ways. In most of our own research laboratories, university or institute based, I imagine we have hosted the same range of nationalities of researchers from all over the world that my Laboratory of Structural Chemistry in Manchester has had these last 25 years. It is worth highlighting I think the ICSU (International Council for Scientific Unions) policy under which all our crystallography conferences are held namely the ‘free circulation of scientists’ [41]. This seeks to ensure that the whole World can benefit from scientific research and create a sustainable future for all based on scientific research wherever possible.

Suffice to say crystallography is one of the most inter disciplinary of the sciences and I believe we have much to contribute to the very wide issues and challenges that sustainability presents. As a research community, and also our leaders, we have made major contributions to the sustainability goals described above in the past and we can do so in the future.

6. ACKNOWLEDGEMENTS

I am grateful to Dr Cora Lind-Kovacs (Univ. of Toledo) and Professor Robin D. Rogers (McGill University), organisers of the ACA 2015 Transactions Symposium, for their constructive comments to me on writing this manuscript. I am also grateful to Brian McMahon and Peter Strickland of the IUCr in Chester, UK for their suggestions and indeed also our work together over many years involving data and publication.

7. REFERENCES

- 1 <http://en.wikipedia.org/wiki/Sustainability> Last Accessed July 19, 2015.
- 2 <http://www.ecu.ac.uk/equality-charters/athena-swan/> Last Accessed July 19, 2015.
- 3 H. Kamminga *Acta Cryst.* **A45** (1989), 581.
- 4 C.J. LeRoy *Science.* **348** (2015) 511.
- 5 <http://iycr2014.org/about/video> Last Accessed July 19, 2015.
- 6 <http://iycr2014.org/about/promotional-materials> Last Accessed July 19, 2015.
- 7 http://iycr2014.org/events/activities_for_schoolchildren Last Accessed July 19, 2015.
- 8 <http://www.icsu.org/> Last Accessed July 19, 2015.
- 9 <http://www.codata.org/> Last Accessed July 19, 2015.
- 10 <http://www.icsti.org/> Last Accessed July 19, 2015.
- 11 H. Hackmann <http://www.aaas.org/event/15th-annual-barnard-lecture> Last Accessed July 19, 2015.
- 12 <https://www.stfc.ac.uk/stfc/cache/file/4304D848-4E42-468A-89984CE70C5CB565.pdf> Last Accessed July 19, 2015.

- 13 E.J. Maclean, P.J. Rizkallah and J.R. Helliwell *European Pharmaceutical Review* (2006), Issue 2, 71.
- 14 <http://www.codata.org/nanomaterials> Last Accessed July 19, 2015.
- 15 <http://www.icsu.org/general-assembly/news/ICSU%20Report%20on%20Open%20Access.pdf> Last Accessed July 19, 2015.
- 16 <http://scitation.aip.org/content/aca/journal/sdy;jsessionid=5tjl1i61uv67r.x-aip-live-03> Last Accessed July 19, 2015.
- 17 D. W. J. Cruickshank (1924-2007) Obituary:- <http://journals.iucr.org/a/issues/2007/05/00/es0361/es0361.pdf> Last Accessed July 19, 2015.
- 18 D. W. J. Cruickshank *Acta Cryst.* **D55** (1999), 583.
- 19 M. Gurusaran, M. Shankar, R. Nagarajan, J.R. Helliwell & K. Sekar *IUCrJ*, 1 (2014), 74.
- 20 K.S.D. Kumar, M. Gurusaran, S.N. Satheesh, P. Radha, S. Pavithra, K.P.S. Thulaa Tharshan, J.R. Helliwell, J.R. & K. Sekar *J. Appl. Cryst.* **48** (2015), 939.
- 21 B. McMahon *Data Science J.*, **1** (2002), 54.
- 22 <http://forums.iucr.org/viewtopic.php?f=21&t=343> Last Accessed July 19, 2015.
- 23 S.W.M. Tanley, A.M.M. Schreuers, J.R. Helliwell, L.M.J. Kroon-Batenburg *J. Appl. Cryst.* **46** (2013), 108.
- 24 Loes M. J. Kroon-Batenburg and John R. Helliwell *Acta Cryst.* **D70** (2014), 2502.
- 25 T.C. Terwilliger *Acta Cryst.* **D70** (2014), 2500.
- 26 T.C. Terwilliger & G. Bricogne *Acta Cryst.* **D70** (2014), 2533.
- 27 L.M.J. Kroon-Batenburg & J.R. Helliwell *Acta Cryst.* **D70** (2014), 2502.
- 28 J.M. Guss & B. McMahon *Acta Cryst.* **D70** (2014), 2520.
- 29 G. R. Meyer, D. Aragão, N. J. Mudie, T. T. Caradoc-Davies, S. McGowan, P. J. Bertling, D. Groenewegen, S. M. Quenette, C. S. Bond, A. M. Buckle and S. Androulakis *Acta Cryst.* **D70** (2014), 2510.
- 30 <http://grants.nih.gov/grants/guide/rfa-files/RFA-MD-15-005.html> Last Accessed July 19, 2015.
- 31 <http://www.library.manchester.ac.uk/services-and-support/staff/research/services/manchester-escholar/> Last Accessed July 19, 2015.
- 32 http://www.chemistry.manchester.ac.uk/media/eps/schoolofchemistry/aboutus/athenaswan/pdf/ManchesterChemistry_AthenaSWAN_Application_BronzeAward.pdf Last Accessed July 19, 2015.
- 33 K. Lonsdale *Is Peace possible?* (Penguin books, London 1957). <https://archive.org/details/ispeacepossible00lons> Last Accessed July 19, 2015.
- 34 <http://pugwash.org/> Last Accessed July 19, 2015.
- 35 L. Pauling *The nature of the chemical bond and the structure of molecules and crystals; an introduction to modern structural chemistry* (3rd ed.) (Cornell University Press, Ithaca (NY): 1960)
- 36 L. Pauling *No more War!* (Dodd, Mead and Company, New York 1958)
- 37 W. Shakespeare *Hamlet* 1603.
- 38 W. van der Kloot *Notes Rec. R. Soc.* **59** (2005), 273.
- 39 <http://sesame.org.jo/sesame/about-us/historical-highlights/2004-foundation-of-a-synchrotron-light-source-in-the-middle-east.html> Last Accessed July 19, 2015.
- 40 <http://www.esrf.eu/home/events/conferences/2015/afls-conference.html>
- 41 <http://www.icsu.org/freedom-responsibility/cfrs/statute-5> Last Accessed July 19, 2015.

**THE TWO-STEP HYDROTHERMAL METHOD:
AN EFFECTIVE APPROACH FOR THE CRYSTAL GROWTH OF NEW MATERIALS
CONTAINING METALS IN REDUCED OXIDATION STATES**

Dileka Abeysinghe, Anthony J. Cortese, Jeongho Yeon and Hans-Conrad zur Loye
Department of Chemistry and Biochemistry, University of South Carolina, Columbia, SC
29208

ABSTRACT

Materials discovery via crystal growth is an active area of research that has led to the preparation of many novel materials along with the determination of their crystal structures. One sub-area of this field is the preparation of organic/inorganic hybrid materials containing metals in reduced oxidation states. Our group has established two new synthetic routes for the efficient preparation of new reduced systems, including 1) a low temperature two-step hydrothermal method and 2) a high temperature molten flux method. The two-step approach, where the reduction of the metal cations is performed in a first step and the crystal growth is performed in a second step, can lead to vastly improved yield in certain situations. In this paper the two-step hydrothermal method is highlighted and, using several compositions that have been prepared via this approach as examples, the advantages of the method are illustrated. The two-step approach is contrasted with the more traditional one-step method and the situations where the use of the two-step approach is advantageous are described.

INTRODUCTION

For the past several years there has been a sustained effort to create new synthetic techniques that focus on sustainable and green synthetic approaches to prepare new materials. In our preparation of new reduced hybrid materials, we have developed a method that is both environmentally friendly and sustainable as it uses renewable, nontoxic reducing agents. Simple organic carboxylic acids are far less hazardous in comparison to reagents traditionally used to perform reductions. For example Zn amalgam requires the use of mercury, Na amalgam is hazardous and requires the use of environmentally unfriendly organic solvents, and HF is very toxic and requires extra ventilation. For these reasons we have chosen to use naturally occurring organic carboxylic acids, such as oxalic acid and tartaric acid, as reducing agents. Both satisfactorily perform the reduction of V(V) to V(IV) under mild hydrothermal conditions. Further, by using reusable reaction vessels, water as a solvent, and earth abundant elements, our chemistry is both sustainable and environmentally friendly.

The synthesis of new materials containing metals in reduced oxidation states is a relatively unexplored area of research due to the difficulties associated with stabilizing and incorporating reduced metal centers into both strictly inorganic as well as organic/inorganic hybrid materials. In particular in the field of crystal growth, establishing and maintaining reducing conditions can be rather difficult depending on the specific method used. Historically, a number of different crystal growth approaches have been explored for the growth of materials containing metals in

reduced oxidation states, including fused salt electrolysis [1-3], chemical vapor transport [4], flux [5-11], and hydrothermal methods [12,13]. These at times onerous approaches have managed to address and overcome a variety of synthetic challenges, including the sensitivity of the reduced compounds to air and moisture, or the, at times, inability to obtain single phase products.

The use of mild hydrothermal or mild solvothermal routes for crystal growth have become popular recently due to the ease with which single crystals of new compositions can be obtained, albeit, rarely containing metals in reduced oxidation states. We have explored this approach because relative to the previously mentioned methods, it appears to be easier to use and enjoys a high success rate in the formation of single crystals. As detailed below, sometimes the crystals that grow are not the desired product and for that reason we have modified this method and have developed the low temperature two-step hydrothermal method for creating crystals containing metals in reduced oxidations states [14-17]. This approach is particularly useful for systems where the *in situ* reduction is kinetically too slow versus the crystallization of an unwanted fully oxidized species. Using several examples, we will illustrate the advantages of the two-step method in this review.

Mild hydrothermal synthesis in which reactions are performed in the subcritical regime at moderate temperatures (<250 °C) and autogenous pressures has been extensively used for crystal growth in recent years due to its simplicity, cost effectiveness, and materials consideration compared to conventional high temperature and high pressure hydrothermal methods [18-23]. Either poly(tetrafluoroethylene) (PTFE) Teflon-lined autoclaves or Pyrex tubes can be used as reaction vessels for these types of reactions. In addition, to avoid the need for a large number of reaction vessels, the “Teflon-pouch technique” was introduced by Poeppelmeier, which involves multiple Teflon [floro(ethylene-propylene)] (FEP) pouches being placed inside a single, larger sized pressure vessel [22]. Both Pyrex and PTFE are suitable materials to serve as reaction vessels for the preparation of reduced materials since they provide the necessary redox neutral environment.

Typically, a reduction can be performed in two different ways: starting with metals already in the desired low oxidation state or using a reducing agent targeting *in situ* reduction. In the former case, using a metal precursor in the desired reduced oxidation state is convenient, however, synthesis conditions must be adjusted to preserve the reduced oxidation state. In the latter case, it is well known that a variety of organic species including polyols, acetates, oxalic acid, and tartaric acid [14-17, 24-26] as well as inorganic species including Zn amalgam, HI [27,28], and HF [18-20] can function as reducing agents to create reduced metal cations in solution as well as functioning to maintain reducing conditions during the entire reaction process. This is rather convenient, however, there are situations where kinetic considerations enter the picture and prevent the formation of the desired product. Specifically, if the rate of reduction of the metal cation is slow relative to the crystallization of the cation with other reagents, then the reaction will result in the creation of an unwanted oxidized species. We have observed this in a number of instances, which prompted us to create the two-step mild hydrothermal method, where the reduction step is separated in time from the crystal growth step, thereby preventing this issue from interfering with the formation of the desired product. In addition, the reducing agent

remaining in the system assures that during the crystal growth step the reaction remains in a reducing environment.

Example 1. $\text{Cs}_2\text{V}_3\text{O}_8$

Vanadates that crystallize in the Fresnoite-type structure have been extensively studied because several of them exhibit low dimensional magnetic behavior. This structure type has the compositions $\text{A}_2\text{MM}'_2\text{O}_8$ ($\text{A} = \text{Sr}^{2+}$ or Ba^{2+} , $\text{M} = \text{Ti}^{4+}$, and $\text{M}' = \text{Si}^{4+}$ or Ge^{4+}) and consists of a two-dimensional layered-type crystal structure [29-31]. The tetravalent titanium, silicon or germanium can be substituted for by either V(IV) or V(V) cations, due to their very similar ionic sizes [32], and several vanadates with composition $\text{A}_2\text{V}_3\text{O}_8$ ($\text{A} = \text{K}$, Rb , or NH_4) have been synthesized and studied for their magnetic properties. The fact that the cesium composition had not been reported prompted us to investigate its synthesis. The other vanadates had been synthesized via a number of routes, including flux reactions and conventional solid state syntheses [32-35], all performed above 500 °C. Our initial attempts to prepare $\text{Cs}_2\text{V}_3\text{O}_8$ by modifying the reported synthetic routes failed, prompting us to investigate low temperature mild hydrothermal synthesis. Using V_2O_5 , Cs_2CO_3 , and oxalic acid as our starting materials we performed the hydrothermal synthesis at 200 °C. Oxalic acid is known to be a mild reducing agent that is able to reduce V(V) to V(IV). These reaction conditions and various permutations resulted inevitably in the formation of an unidentified phase (major product), CsVO_3 (major product), and $\text{Cs}_2\text{V}_3\text{O}_8$ (minor product). On the one hand, this reaction was a success as we obtained the desired product; on the other hand, the yield of brown $\text{Cs}_2\text{V}_3\text{O}_8$ crystals was very poor and unsatisfactory. Nonetheless, even with poor yield, we were able to solve the single crystal structure of $\text{Cs}_2\text{V}_3\text{O}_8$, shown in Figure 1.



Figure 1. Optical image of single crystals of $\text{Cs}_2\text{V}_3\text{O}_8$. Crystals are ~ 0.2 mm in length.

$\text{Cs}_2\text{V}_3\text{O}_8$ crystallizes in space group $P4bm$ and exhibits a layered structure type consisting of sheets of corner shared VO_4 tetrahedra and VO_5 square pyramids. The VO_5 square pyramids are separated from each other by V_2O_7 groups creating $\text{V}_3\text{O}_8^{2-}$ layers in the ab plane. As can be seen in Figure 2, the cesium atoms are located between the layers and provide charge balance. The composition indicates that $\text{Cs}_2\text{V}_3\text{O}_8$ contains two V(V) and one V(IV) cation. Based on bond valence analysis, V(V) is found in VO_4 tetrahedra, while V(IV) is located in VO_5 square pyramids.

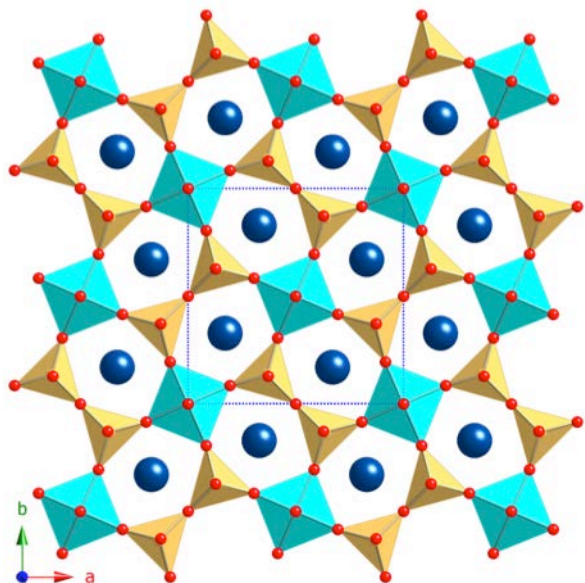


Figure 2. $\text{Cs}_2\text{V}_3\text{O}_8$ extended structure representation along the c axis. Vanadium in VO_4 tetrahedra, vanadium in VO_5 square pyramids, cesium, and oxygen are shown in yellow, cyan, blue, and red, respectively.

The problem that remained was the poor yield of the reaction as one of the goals had been to carry out magnetic measurements on this potentially low-dimensional magnetic material. One of the problems was the formation of CsVO_4 , containing V(V). This suggested that the formation of CsVO_4 was fast relative to the reduction of V(V) to V(IV) by the oxalic acid and the subsequent crystallization of $\text{Cs}_2\text{V}_3\text{O}_8$. To solve this problem, we devised the two-step hydrothermal method where we separated the hydrothermal route into two sequential steps: 1) the reduction of the vanadium precursor and 2) the reaction of the reduced vanadium species with cesium. Step one consisted of heating a mixture of 1 mmol of V_2O_5 , 1.5 mmol of $\text{H}_2\text{C}_2\text{O}_4 \cdot 2\text{H}_2\text{O}$ and 1 mL of H_2O in a 23 mL Teflon-lined autoclave and heating the mixture to 150 °C for 12 h. Once cooled, the autoclave was opened and 2 mmol of Cs_2CO_3 were added to the product from the first reaction, which consisted of dark brown solids suspended in a blue solution. Repeating the heating process at 150 °C for 24 h resulted in product consisting of deep brown single crystals of $\text{Cs}_2\text{V}_3\text{O}_8$ along with unidentified impurities that were removed by sonication. The yield was approximately 91% based on V_2O_5 .

The fact that the V(IV) is restricted to the layers that in turn are isolated from each other by the cesium cations suggests that low dimensional magnetic behavior might be present. For that reason the magnetic susceptibility data were measured as a function of the temperature. The effective magnetic moment for V(IV) was 1.78 μB , consistent with what had been found for other V(IV) species. Short-range magnetic ordering was observed around 7 K and the susceptibility data were fit to the Heisenberg square lattice model, which supported the existence of short-range antiferromagnetic and two-dimensional magnetic interactions [15].

The ability to create conditions where the reduced vanadium solution species was able to react directly with the cesium enabled us to obtain the desired $\text{Cs}_2\text{V}_3\text{O}_8$ product in good yield and allowed us to measure its magnetic properties. The observations made here are not unique and similar issues can be observed in other systems, as detailed in the following sections.

Example 2. $\text{Ba}_3[(\text{VO})_2(\text{C}_2\text{O}_4)_5(\text{H}_2\text{O})_6]\cdot(\text{H}_2\text{O})_3$,

Our interest in vanadium containing compounds is prompted by the potentially very interesting magnetic properties as well as by the goal of creating organic inorganic hybrid materials containing reduced vanadium in the structure. As mentioned in the previous section, oxalic acid is a mild reducing agent quite sufficient for creating V(IV) species in solution, and also a chelating agent that can aid in the formation of organic/inorganic hybrid materials. Mild hydrothermal synthesis had been shown to be effective for creating organic/inorganic hybrid materials containing reduced metal cations. We decided to use the oxalic acid as an *in situ* reducing agent as well as a complexing agent. To prepare new complex vanadium oxalates, we attempted the reaction of V_2O_5 , $\text{H}_2\text{C}_2\text{O}_4\cdot 2\text{H}_2\text{O}$, $\text{Ba}(\text{OH})_2\cdot 8\text{H}_2\text{O}$, and H_2O at $160\text{ }^\circ\text{C}$ in a Teflon lined autoclave. After a 24 h heating cycle, the result was barium oxalate, BaC_2O_4 , as the predominant crystalline product. Clearly, the reaction between oxalic acid and V_2O_5 was too slow relative to the fast precipitation of BaC_2O_4 . To avoid the formation of BaC_2O_4 , we again used the two-step mild hydrothermal method and this time reacted 1 mmol of V_2O_5 , 4 mmol of $\text{H}_2\text{C}_2\text{O}_4\cdot 2\text{H}_2\text{O}$, and 4 mL of H_2O in the PTFE autoclave at $160\text{ }^\circ\text{C}$ for 12 hrs. Once everything had cooled down to room temperature the autoclave contained a blue solution to which 1 mmol of $\text{Ba}(\text{OH})_2\cdot 8\text{H}_2\text{O}$ were added. The heating profile was repeated at $160\text{ }^\circ\text{C}$ for 48 h. This resulted in blue $\text{Ba}_3[(\text{VO})_2(\text{C}_2\text{O}_4)_5(\text{H}_2\text{O})_6]\cdot(\text{H}_2\text{O})_3$ crystals, shown in Figure 3, in approximately 90% yield based on V_2O_5 .



Figure 3. Optical image of single crystals of $\text{Ba}_3[(\text{VO})_2(\text{C}_2\text{O}_4)_5(\text{H}_2\text{O})_6]\cdot(\text{H}_2\text{O})_3$. Crystals are ~ 0.5 mm in length.

$\text{Ba}_3[(\text{VO})_2(\text{C}_2\text{O}_4)_5(\text{H}_2\text{O})_6]\cdot(\text{H}_2\text{O})_3$ crystallizes in the monoclinic space group $C2/c$ and exhibits a 3D framework structure in which distorted VO_6 octahedra and irregular $\text{BaO}_{11}/\text{BaO}_{12}$ polyhedra are bridged by oxalate ligands. The structure is shown in Figure 4 highlighting the Ba/V oxalate connectivity that generates channels along the $[101]$ direction. The channels are filled with both interstitial and coordinated water molecules. The vanadium is located in distorted VO_6 octahedra, where four of the six oxygens originate from two bidentate oxalate ligands, one from a monodentate oxalate and one from a bridging oxygen (oxo) atom. These units are linked via one oxalate ligand to create V_2O_{12} dimers. These dimers connect with each other via Ba atoms to create the extended framework structure.

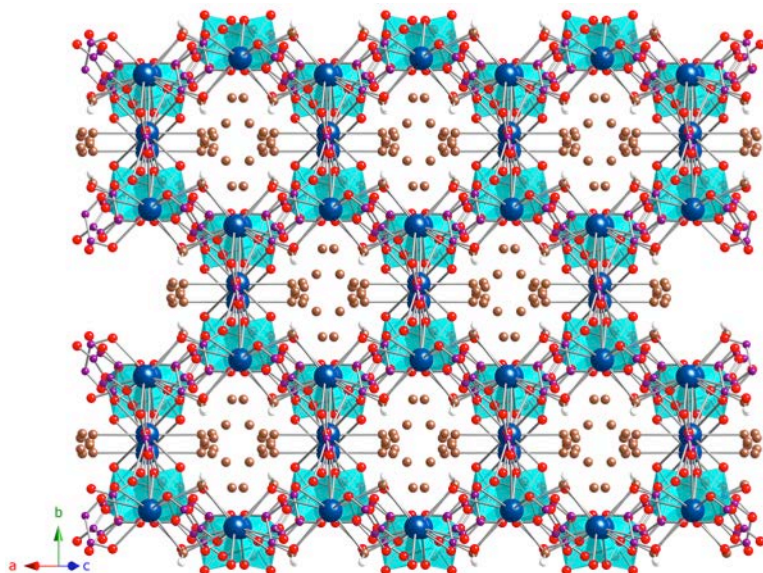


Figure 4. Ba/V oxalate connectivity of $\text{Ba}_3[(\text{VO})_2(\text{C}_2\text{O}_4)_5(\text{H}_2\text{O})_6]\cdot(\text{H}_2\text{O})_3$ generates channels running along the [101] direction. Vanadium, barium, carbon, oxygen are shown in cyan, blue, purple, red, respectively. Water molecules shown in brown and white.

Since the channels contain water molecules, it is reasonable to see if they can be removed by heating the materials and, furthermore, if this can be accomplished while retaining the crystallinity of the material. The low temperature removal of some of the interstitial and coordinated waters present in the channels resulted in two new compounds, $\text{Ba}_3[(\text{VO})_2(\text{C}_2\text{O}_4)_5(\text{H}_2\text{O})_4]\cdot(\text{H}_2\text{O})_2$, **2**, and $\text{Ba}_3[(\text{VO})_2(\text{C}_2\text{O}_4)_5(\text{H}_2\text{O})_2]$, **3**, that were created via a crystal-to-crystal transformation at 50 °C (or vacuum for 12 h) and 100 °C, respectively, after heating for 12 h (Figure 5). The structure of compound **2**, which crystallizes in the monoclinic space group $C2/c$, is very similar to the parent structure having lost one of the interstitial and two of the coordinated water molecules. Heating **2** results in the loss of an additional four water molecules, two interstitial and two coordinated, and the formation of compound **3**, which crystallizes in the monoclinic space group $P2_1/c$. While the crystal-to-crystal transformation of **1** to **2** is reversible, the crystal-to-crystal transformation of **1** to **3** is irreversible. Having lost seven water molecules, all interstitial and four coordinated water molecules, makes the structure of the compound **3** unique in that the channels are no longer present.

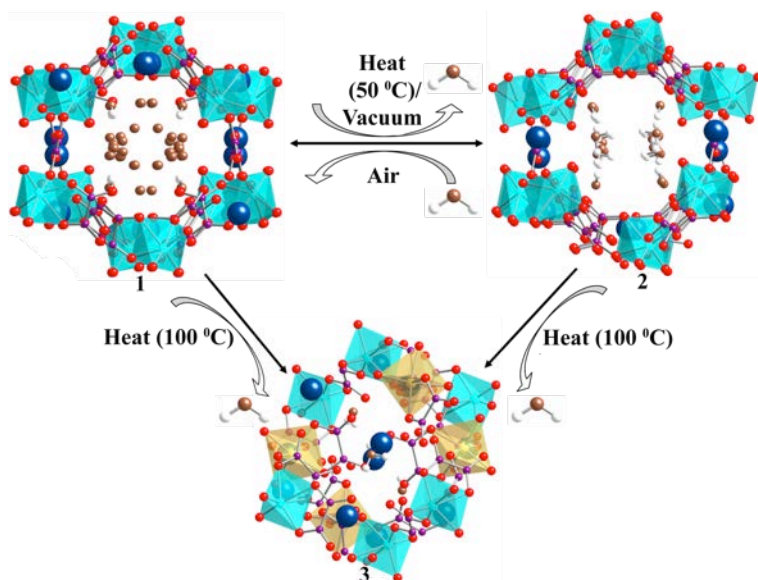


Figure 5. Crystal-to-crystal transformation from $\text{Ba}_3[(\text{VO})_2(\text{C}_2\text{O}_4)_5(\text{H}_2\text{O})_6] \cdot (\text{H}_2\text{O})_3$ (**1**), to $\text{Ba}_3[(\text{VO})_2(\text{C}_2\text{O}_4)_5(\text{H}_2\text{O})_4] \cdot (\text{H}_2\text{O})_2$ (**2**), and $\text{Ba}_3[(\text{VO})_2(\text{C}_2\text{O}_4)_5(\text{H}_2\text{O})_2] \cdot (\text{H}_2\text{O})_2$ (**3**).

The main reason for the loss of the channels is the absence of water molecules, which permits the rotation of the two vanadium centers in **3** that closes the channel. Throughout the transformation from **1** to **2** to **3**, the color of the crystals as well as the oxidation state of vanadium, +4, remains unchanged, demonstrating exceptional crystal stability.

Example 3. $\text{A}_2[(\text{VO})_2(\text{C}_4\text{H}_2\text{O}_6)_2(\text{H}_2\text{O})_2] \cdot (\text{H}_2\text{O})_2$ (A = K, Rb, and Cs)

The two-step mild hydrothermal method described above involved running the reaction twice, once to carry out the reduction and once to perform the crystal growth. It is not, however, necessary to carry out the reduction in the actual reaction vessel, as it is possible, and often desirable, to prepare stock solutions containing the reduced species or to prepare the solution containing the reduced cation in one reaction vessel, but to carry out the crystal growth step using a different reaction vessel. Vanadium can exist in multiple oxidation states in solution, ranging from +2 to +5 with the colors yellow (V^{5+}), blue (V^{4+}), green (V^{3+}), and lilac (V^{2+}) (Figure 6). $\text{V}(\text{IV})$ can readily be generated using mild organic reducing agents while stronger reducing agents, such as zinc, are needed to create $\text{V}(\text{II})$ species. For the synthesis of $\text{A}_2[(\text{VO})_2(\text{C}_4\text{H}_2\text{O}_6)_2(\text{H}_2\text{O})_2] \cdot (\text{H}_2\text{O})_2$ (A = K, Rb, and Cs), tartaric acid was used as the reducing agent and in the first step, 1 mmol of V_2O_5 , 4 mmol of L-(+)- $\text{C}_4\text{H}_6\text{O}_6$, and 4 mL of H_2O were placed in a PTFE autoclave and heated to $160\text{ }^\circ\text{C}$ for 4 h. Once cooled to room temperature, the blue solution was transferred to a thick walled PTFE capped Pyrex tube and combined with 2 mmol of Cs_2CO_3 and 3 mmol of CsCl . This mixture was heated at $90\text{ }^\circ\text{C}$ for 48 h. Decanting the mother liquor left the single crystalline product behind. The yield of the reaction was $\sim 85\%$ based on V_2O_5 . The potassium and rubidium analogs were obtained via the same procedure the only difference being the use of potassium and rubidium instead of cesium salts and simple alcohols, methanol (1.0 mL) and ethanol (2.7 mL), respectively. Figure 7 shows the optical images of potassium, rubidium, and cesium compounds.

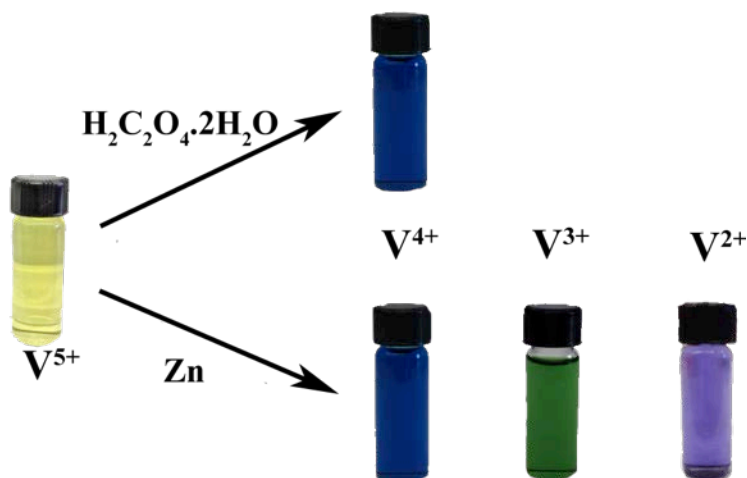


Figure 6. Colors of vanadium's oxidation states in the solution.

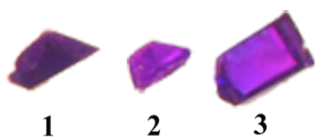


Figure 7. Optical images of single crystals of $\text{K}_2[(\text{VO})_2(\text{C}_4\text{H}_2\text{O}_6)_2(\text{H}_2\text{O})_2] \cdot (\text{H}_2\text{O})_2$, **1**, $\text{Rb}_2[(\text{VO})_2(\text{C}_4\text{H}_2\text{O}_6)_2(\text{H}_2\text{O})_2] \cdot (\text{H}_2\text{O})_2$, **2**, and $\text{Cs}_2[(\text{VO})_2(\text{C}_4\text{H}_2\text{O}_6)_2(\text{H}_2\text{O})_2] \cdot (\text{H}_2\text{O})_2$, **3**. Crystals are ~ 0.75 mm in length.

The rubidium and cesium containing tartrates are isostructural. They both crystallize in the chiral, orthorhombic space group $P2_12_12_1$ and form in a 3D crystal structure consisting of distorted VO_6 octahedra and irregular $\text{AO}_9/\text{AO}_{10}$ ($A = \text{Cs}, \text{Rb}$) polyhedra that are linked via bridging tartrate ligands. The extended structure viewed along the a axis is shown in Figure 8. The vanadium VO_6 octahedra are highly distorted with four equatorial V-O bonds of roughly the same length, one exceptionally long V-O axial bond, and one exceptionally short V-O bond. Two bidentate tartrate ligands provide four of the six oxygens, and the other two are from a water ligand and one bridging oxygen (oxo) atom. The two VO_6 distorted octahedra are connected into the dimeric units shown in Figure 9 via the bidentate tartrate ligands. Cesium or rubidium cations further connect these dimers and create the extended structure.

The potassium-containing compound crystallizes in a different structure in the orthorhombic space group $C222_1$. Its 3D structure consists of VO_6 distorted octahedra, VO_5 square pyramids, and KO_7/KO_8 irregular polyhedra linked via bridging tartrate ligands. The extended structure viewed down the a axis is shown in Figure 10. The origin of the structural difference is due to the different protonation patterns of the tartrate ligands. While the ligand in the potassium phase is fully protonated, the rubidium and cesium containing phases contain tartrate ligands that are only partially deprotonated.

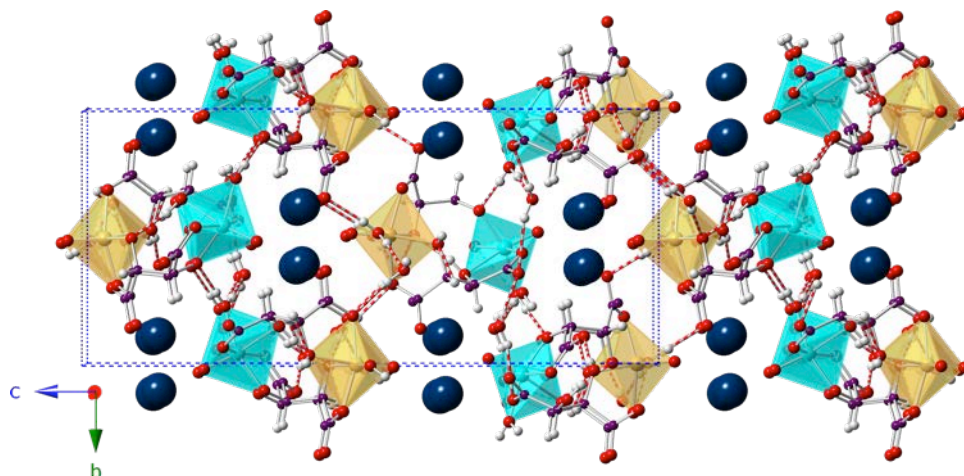


Figure 8. $A_2[(VO)_2(C_4H_2O_6)_2(H_2O)_2] \cdot (H_2O)_2$ ($A = Rb$ and Cs) structure representation along the a axis. Two different vanadium polyhedra are shown in cyan and yellow. Cesium/rubidium, carbon, oxygen, and hydrogen are shown in blue, purple, red, white, respectively. Hydrogen bonds are shown in red and white cylinders.

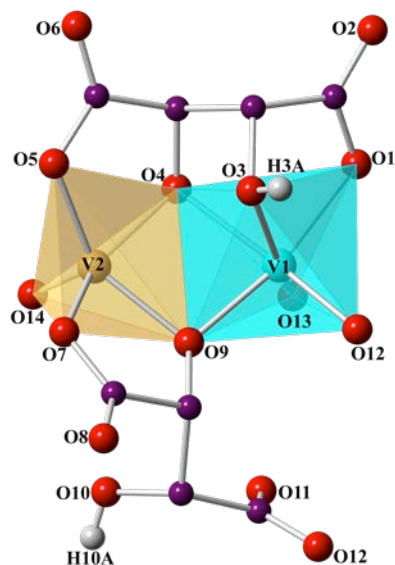


Figure 9. V_2O_9 dimers of $K_2[(VO)_2(C_4H_2O_6)_2(H_2O)_2] \cdot (H_2O)_2$.

The potassium phase contains unique edge sharing V_2O_9 dimers that are created by edge sharing of VO_6 distorted octahedra and VO_5 square pyramids. This structure of the edge sharing dimers is such that the two vanadium V(IV) cations are relatively close to each other and, as a result, their spins interact magnetically. This is in contrast to the other two phases in which the vanadium V(IV) cations are too far apart to allow for any spin coupling. This is supported by magnetic measurements that resulted in paramagnetic behavior for the rubidium and cesium phases and interesting spin dimer behavior for the potassium phase [17]. Finally, due to the fact that all three crystallize in non-centrosymmetric space groups, they were tested and found to be second harmonic generation active.

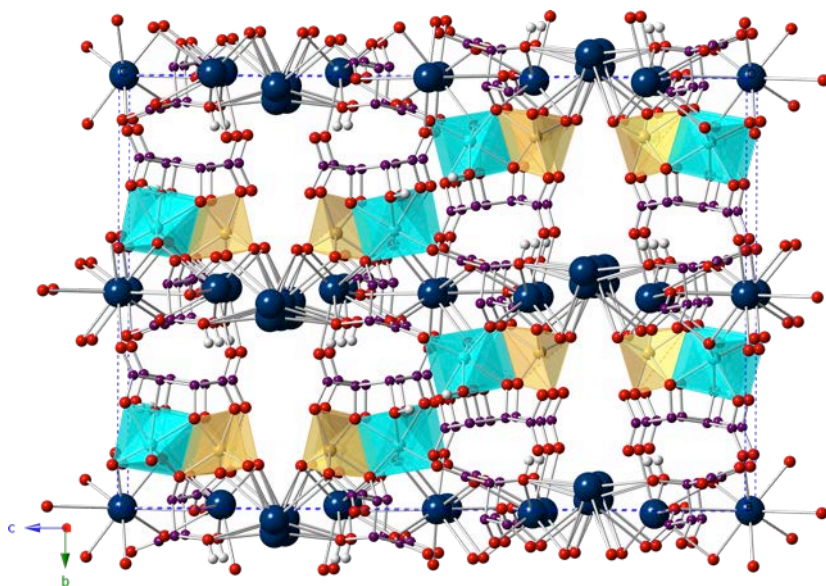


Figure 10. $K_2[(VO)_2(C_4H_2O_6)_2(H_2O)_2] \cdot (H_2O)_2$ structure representation along the a axis. (K is shown in blue, colors of the rest of the atoms are same as Rb/Cs structure.)

SUMMARY

Using a two-step mild hydrothermal method we were able to grow crystals of several new V(IV) containing materials, including pure inorganic structures as well as organic/inorganic hybrid materials. This approach is general and, although not discussed in this paper, can be used for the preparation of a wide variety of systems, including oxy-hydroxides, fluorides and oxy-fluorides. Furthermore, the use of nontoxic and renewable reducing agents, reusable reaction vessels, earth abundant elements, and water as solvent, makes this method more sustainable and environmental friendly. The ability to prepare stock solutions containing metal cations in pre-selected oxidation states makes it possible to target products containing metal cations in specific oxidation states. The main advantage of this method is in cases where, for kinetic reasons, the desired product is slow to crystallize and as a result the reaction yields unwanted products.

ACKNOWLEDGEMENTS

Financial support through the National Science Foundation under award DMR-1301757 is gratefully acknowledged.

REFERENCES

- [1] C.R. Feger, R.P. Ziebarth, *Chem. Mater.* **7** (1995), 373.
- [2] A. Moini, M.A. Subramanian, A. Clearfield, F.J. DiSalvo, W.H. McCarroll, *J. Solid State Chem.* **66** (1987), 136.
- [3] C.C. Torardi, C. Fecketter, W.H. McCarroll, F.J. DiSalvo, *J. Solid State Chem.* **60** (1985), 332.
- [4] M.L. Gray, R. Kershaw, W. Croft, K. Dwight, A. Wold, *J. Solid State Chem.* **62** (1986), 57.
- [5] P.P. Tsai, J.A. Potenza, M. Greenblatt, *J. Solid State Chem.* **69** (1987), 329.
- [6] M. Greenblatt, *Chem. Rev.* **88** (1988), 31.
- [7] M. Greenblatt, *Phys. Chem. Mater. Low-Dimension. Struct.* **11** (1989), 1.
- [8] B. Hessen, S.A. Sunshine, T. Siegrist, R. Jimenez, *Mater. Res. Bull.* **26** (1991), 85.

- [9] B. Hessen, S.A. Sunshine, T. Siegrist, A.T. Fiory, J.V. Waszczak, *Chem. Mater.* **3** (1991), 528.
- [10] D.L. Serra, S.-J. Hwu, *J. Solid State Chem.* **101** (1992), 32.
- [11] D. Abeyasinghe, B. Gerke, G. Morrison, C.H. Hsieh, M.D. Smith, R. Pöttgen, T.M. Makris, H.-C. zur Loye, *J. Solid State Chem.* **229** (2015), 173.
- [12] Y. Oka, T. Yao, N. Yamamoto, M. Ueda, S. Maegawa, *J. Solid State Chem.* **149** (2000), 414.
- [13] Y. Oka, T. Yao, N. Yamamoto, Y. Ueda, A. Hayashi, *J. Solid State Chem.* **105** (1993), 271.
- [14] J. Yeon, M.D. Smith, A.S. Sefat, H.-C. zur Loye, *Inorg. Chem.* **52** (2013), 2199.
- [15] J. Yeon, A.S. Sefat, T.T. Tran, P.S. Halasyamani, H.-C. zur Loye, *Inorg. Chem.* **52** (2013), 6179.
- [16] D. Abeyasinghe, M.D. Smith, J. Yeon, G. Morrison, H.-C. zur Loye, *Cryst. Growth Des.* **14** (2014), 4749.
- [17] A.J. Cortese, B. Wilkins, M.D. Smith, J. Yeon, G. Morrison, T.T. Tran, P.S. Halasyamani, H.-C. zur Loye, *Inorg. Chem.* **54** (2015), 4011.
- [18] J. Yeon, M.D. Smith, J. Tapp, A. Möller, H.-C. zur Loye, *Inorg. Chem.* **53** (2014), 6289.
- [19] J. Yeon, M.D. Smith, J. Tapp, A. Moller, H.-C. zur Loye, *J. Am. Chem. Soc.* **136** (2014), 3955.
- [20] J. Yeon, M.D. Smith, A.S. Sefat, T.T. Tran, P.S. Halasyamani, H.-C. zur Loye, *Inorg. Chem.* **52** (2013), 8303.
- [21] Y. Chen, T. Liu, C. He, C. Duan, *J. Mater. Chem.* **22** (2012), 19872.
- [22] W.C. Sheets, E. Mugnier, A. Barnabé, T.J. Marks, K.R. Poeppelmeier, *Chem. Mater.* **18** (2006), 7.
- [23] T. Chirayil, P.Y. Zavalij, M.S. Whittingham, *Chem. Mater.* **10** (1998), 2629.
- [24] T. Cochell, A. Manthiram, *Langmuir* **28** (2012), 1579.
- [25] X. Piao, K.- Machida, T. Horikawa, B. Yun, *J. Lumin.* **130** (2010), 8.
- [26] L.H. Kumar, B. Viswanathan, S.S. Murthy, *J. Alloys Compd.* **461** (2008), 72.
- [27] L.R. Morss, *Chem. Rev.* **76** (1976), 827.
- [28] M.J. Polinski, J.N. Cross, E.M. Villa, J. Lin, E.V. Alekseev, W. Depmeier, T.E. Albrecht-Schmitt, *Inorg. Chem.* **52** (2013), 8099.
- [29] T. Höche, C. Rüssel, W. Neumann, *Solid State Commun.* **110** (1999), 651.
- [30] S.A. Markgraf, A. Halliyal, A.S. Bhalla, R.E. Newnham, C.T. Prewitt, *Ferroelectrics* **62** (1985), 17.
- [31] M. Kimura, K. Doi, S. Nanamatsu, T. Kawamura, *Appl. Phys. Lett.* **23** (1973), 531.
- [32] G. Liu, J.E. Greedan, *J. Solid State Chem.* **114** (1995), 499.
- [33] E. Andrukaitis, P.W.M. Jacobs, J.W. Lorimer, *Can. J. Chem.* **68** (1990), 1283.
- [34] M.L. Ha-Eierdanz, U.Z. Mueller, *Z. Anorg. Allg. Chem.* **613** (1992), 63.
- [35] R.L. Withers, T. Höche, Y. Liu, S. Esmailzadeh, R. Keding, B. Sales, *J. Solid State Chem.* **177** (2004), 3316.

USING NEUTRON POWDER DIFFRACTION TO STUDY STRUCTURE FUNCTION RELATIONSHIPS IN ENERGY STORAGE DEVICES¹

Ashfia Huq

*Chemical and Engineering Materials Division,
Oak Ridge National Laboratory, Oak Ridge, TN, United States*

1. ABSTRACT

In electrochemical devices such as fuel cells and batteries, there are materials challenges to make more efficient, cheaper and environment friendly electrodes and electrolytes to compete with fossil fuel performance. Materials development requires a detailed understanding of the structure-property relationship and characterization of lithium, hydrogen or oxygen transport within these systems. Sensitivity to light elements in the presence of heavier elements makes neutron diffraction an ideal tool to study these oxides, hydrides and compounds containing Li. As a result neutron crystallography has been very successfully used to elucidate structures of electrode and electrolyte materials used in both Li-ion batteries and solid oxide fuel cell (SOFC) materials. Some examples where neutron powder diffraction has played the role of unraveling these relationships will be discussed.

2. INTRODUCTION

Electrochemical devices such as fuel cells and batteries have played an enormous role in the advancement of sustainable energy up to the present, and appear poised to enable future mobile technology, effective energy utilization on the grid, and efficient transportation. Improvements made over many decades have resulted in their ubiquitous presence in mobile devices such as laptops, cell phones and other household items [1]. To achieve the goal of a future human civilization that is independent of fossil fuel and can harness the power of wind, water and solar into electrochemical devices for energy storage a tremendous amount of research is still required. There is a clear need to understand the structure-function relationships of both electrode and electrolyte materials under operating conditions. If we can determine the bottlenecks in performance, we can use that knowledge to design better materials. We can also take a holistic approach in system design if we understand the impact of each component on the performance of the device. Historically due to their large penetration depth neutrons have played a significant role in studying processes *in-situ* [2]. The current generation of Li-ion batteries (LIBs) has benefitted greatly from neutron diffraction measurements due to their sensitivity towards Li in the presence of heavier elements and the enhanced contrast between the various transition elements frequently used in candidate cathode materials. A quick search in Web of Science

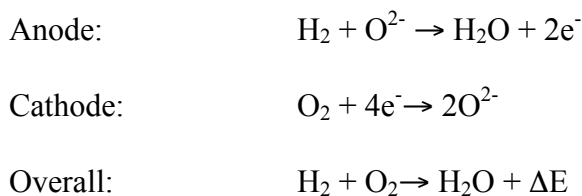
¹ Notice of Copyright

This manuscript has been authored by UT-Battelle, LLC under Contract No. DE-AC05-00OR22725 with the U.S. Department of Energy. The United States Government retains and the publisher, by accepting the article for publication, acknowledges that the United States Government retains a non-exclusive, paid-up, irrevocable, world-wide license to publish or reproduce the published form of this manuscript, or allow others to do so, for United States Government purposes. The Department of Energy will provide public access to these results of federally sponsored research in accordance with the DOE Public Access Plan (<http://energy.gov/downloads/doe-public-access-plan>).

using key words Li ion battery and neutron diffraction brings up over 350 citations. In the case of SOFC electrode materials, a lower operating temperature could extend cell lifetime, reduce material costs, and decrease startup/shutdown times, for which a detailed understanding of oxygen conduction under operational conditions is a prerequisite for progress [3]. The following sections will discuss some examples where neutron powder diffraction has been used as a tool to understand structure function relationships for materials for electrochemistry.

3. *IN-SITU* STUDY OF SOFC MATERIALS

In-situ neutron scattering studies under conditions that simulate the dynamic fuel cell operating environment can provide unique information that cannot be obtained by any other means such as structure; defect location, concentration and ordering; phase transitions as a function of chemical composition, temperature and oxygen partial pressure; phase separation and decomposition; phase behavior in *in-situ* dynamic ion-conducting environments; vibration and diffusion properties of mobile species. These parameters directly determine the cell performance and must be understood in order to move towards intelligent materials design. SOFCs are fabricated as a solid electrochemical chain comprising (fuel|anode|electrolyte|cathode|oxidant). If the electrolyte is an oxygen ion conductor the principal reactions taking place with hydrogen fuel can be summarized as follows



The flow of electronic charge through an outside circuit must be balanced by the flow of ionic charge through the electrolyte and this balance results in generation of electric power. There is considerable research to reduce the operating temperature that ranges from 700-1000 °C. Almost all SOFCs currently being developed employ an yttria-stabilized zirconia, YSZ ($Y_xZr_{1-x}O_2$) electrolyte, a strontium doped lanthanum manganite, LSM ($La_{1-x}Sr_xMnO_3$) as cathode and a mixed nickel/ YSZ cermet anode, and finally doped lanthanum chromate ($LaCrO_3$) as the interconnect between cells.

The key issues for choice of materials are

- Physical and chemical stability in appropriate chemical environment that they are exposed to (oxidizing or reducing ranging from $pO_2 \sim 10^{-18} - 1$ atm). These extreme environments of temperature and pressure can cause phase transitions, formation of phases with huge defects ultimately causing mechanical failure.
- Chemical compatibility and matching thermal conductivity with other components to avoid cracking. It is crucial that the components do not react with each other resulting in formation of different phases or impurity phases that reduce their conductivity and durability.
- From an economic point of view to compete with existing technology the components have to be low cost and easy to fabricate.

While there are established materials that have been commercialized in fuel cells, the search for new and improved materials to reduce the operational temperature, design simpler geometry, and enable direct hydrocarbon conversion continues. For example, both the electrocatalytic activity of the LSM cathode and the ionic conductivity of YSZ electrolyte are too low below 700 °C. Ni cannot be used for dry hydrocarbon fuels as it catalyzes the formation of graphitic coke under these conditions.

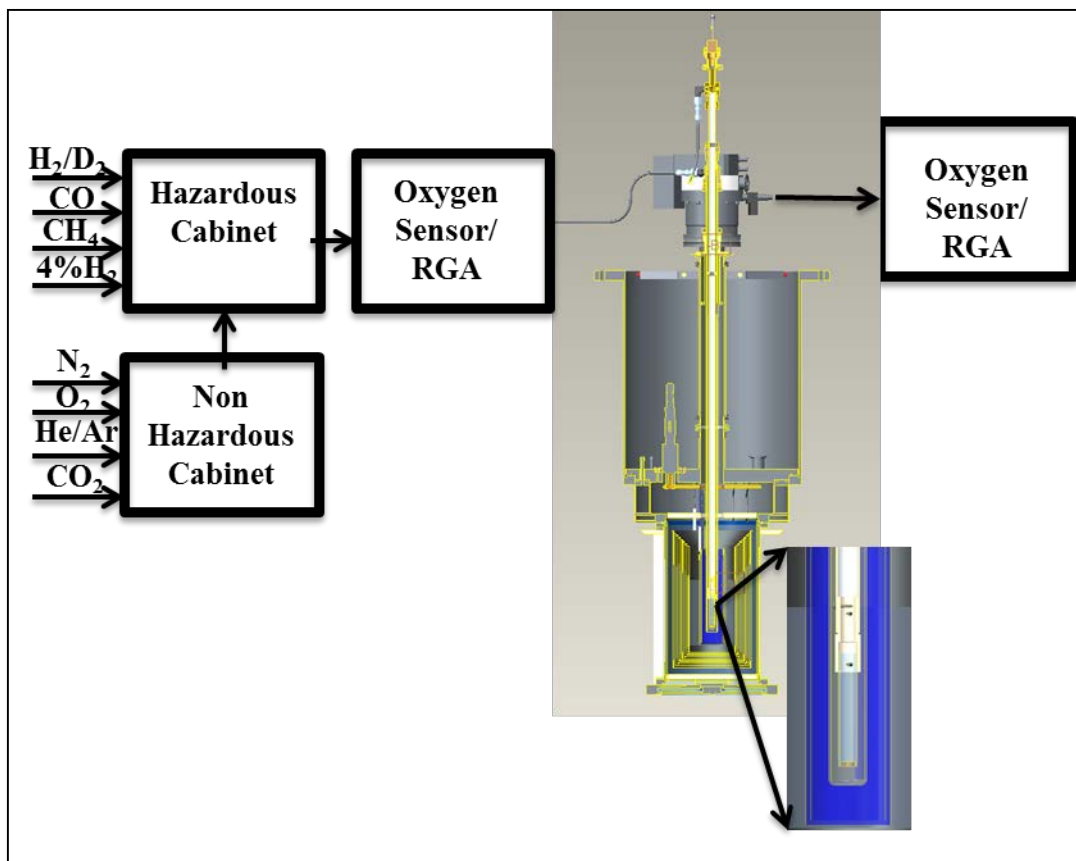


Figure 1. Schematic drawing of the POWGEN furnace and gas handling system. The sample holder is magnified to show how the sample is loaded in the furnace.

While room temperature, *ex-situ* x-ray diffraction had been used routinely by the SOFC community, it often does not tell the whole story as *in-situ* studies are required to understand what occurs under real operating conditions and to map phenomena such as phase stability with respect to temperature and partial pressure of oxygen (pO_2). Traditionally thermogravimetric analysis (TGA) and differential thermal analysis (DTA) are used to monitor change of oxygen content and phase transitions but most of the time it relies on very accurate balances (which require reference systems) and measurements are often not done simultaneously. *In-situ* x-ray measurements are also not very reliable in monitoring the oxygen distribution in the various

crystallographic sites due to the presence of heavier elements which x-rays are more sensitive to. *In-situ* neutron measurements however can solve all of these problems by allowing the measurement of oxygen concentration, crystal structure and phase transitions simultaneously. With these needs in mind, the team at the POWGEN instrument at the Spallation Neutron Source (SNS) located at Oak Ridge National Laboratory (ORNL) in conjunction with a user team led by Dr. Steven McIntosh developed a fully integrated *in-situ* setup to study SOFC materials. This system includes a special quartz insert for gas flow in the traditional ILL vacuum furnace, a gas handling system that can mix several different gases to produce controlled atmospheres in the range $10^{-24} < pO_2 < 1$ atm (using gases from pure H₂ to pure O₂), a commercial residual gas analyzer (RGA) to monitor the incoming gas and a YSZ based oxygen sensor to simultaneously measure the partial pressure of oxygen of the exhaust gas. It should be mentioned here that the RGA and pO₂ sensor are interchangeable so that for catalysis measurements one can monitor the exhaust gas with the RGA. The sample holder is made of quartz with one end open (top) and the bottom made of fritted quartz. The gas flows from the top, through the sample and goes out through the frit.

Using this *in-situ* setup, multiple systems including single perovskites, double perovskites, and RP phases have been studied [4]. In-situ neutron diffraction using the sample environment described above was used to follow the structural evolution of PrBaCo₂O_{5+x} [5] and NdBaCo₂O_{5+x} [6] as a function of temperature (573 to 852 °C) and partial pressure of oxygen ($10^{-4} < pO_2 < 10^{-1}$ atm). Similar behavior was observed for both systems. The primary oxygen vacancies were observed in the Ba plane. For the Pr material, the fractional occupancy of the O-site in the Pr layer ranges between 0.15(1) and 0.53(1). This site also has high anisotropic nuclear displacement in the a-b plane. However the Oxygen site in Co-O plane shows a significantly smaller number of oxygen vacancies with fractional occupancy between 0.976(6) and 0.981(6). Anisotropic nuclear displacement in the c-direction for this site indicates a possible diffusion towards the vacancy-rich Pr layer. The O-site in the Ba layer is, fully occupied (with estimated standard deviations). The detailed analysis of location and displacement of oxygen occupancies describe the transport pathway that is accomplished in these materials by hopping between the vacancy-rich O-site in the Pr layer and the nearest neighbor O-site in the Co layer.

4. RECHARGEABLE BATTERIES

A battery is an electrochemical device made of three primary components: a cathode (an oxidant), anode (a reductant), and electrolyte. During discharge, the electrolyte acts to transfer ionic charge and maintain charge balance while electrons are forced through an external circuit to do electrical work. The ionic mobility of the electrolyte is significantly smaller than the electronic conductivity of the electrodes, and so cells are designed to have relatively large electrode areas compared to the separation of cathode and anode. If the electrolyte is liquid a permeable electrically insulating separator is used to prevent direct reaction between the solid electrodes. Electrode materials are connected to current collectors generally made of the metals Al (cathode) and Cu (anode), which are minimally reactive in their respective voltage windows. The chemical reaction taking place in a rechargeable battery electrode is ideally thermodynamically reversible and kinetically fast. The maximum operational voltage that such a battery can achieve is limited by the energy difference of the HOMO (Highest occupied

molecular orbital) and LUMO (Lowest unoccupied molecular orbital) of the electrolyte. While the battery cells commercialized by SONY Corporation described above have become ubiquitous in our mobile devices, the future challenge lies in the realization of affordable high-power, high-capacity electric vehicles that can compete with cars powered by an internal combustion engine, and stationary storage of electrical energy generated by solar and wind power.

4.1. High Voltage Cathodes

Since the first commercialization of Li ion batteries (LIB), great advances have been made in extending their lifetime. Rechargeable LIBs capable of 30,000 safe cycles, at an acceptable rate of cycling, have been achieved, which translates to a 10 year lifetime. The battery pack used in a NISSAN Leaf or a Tesla Model S is sold with an 8 year warranty. However, for more widespread usage of rechargeable batteries the challenge is to develop a strategy to retain this life time at the same acceptable rate of cycling in a safe fashion but generate a much larger energy density than can be realized with present technologies. The strategies also have to take into account the intended application - for mobile applications such as all-electric vehicles there are gravimetric restrictions and need for large capacities, whereas for stationary applications one needs to store energy at a competitive cost.

The basic idea behind a Li based rechargeable battery is that one requires a cathode that is capable of providing larger voltage vs Li, which was achieved by J.B. Goodenough in 1980 [7,8]. He also realized from his earlier work that while sulfide based cathodes would be limited to ~2.5 V, higher voltages could be achieved using oxides. Around the same time Rachid Yazami's group in France noted that Li could be reversibly intercalated in graphite avoiding the dendrite formation in metal anodes such as Li [9]. This work formed the basis of the commercialization of the first LIB by Akira Yoshino's group in Asahi Chemical, which was later sold to SONY Corporation [10]. The Li and Mn rich (LMR) oxides with chemical formula $\text{Li}_{1+x}\text{M}_{1-x}\text{O}_2$ (M=Ni, Mn, Co) and spinel $\text{LiNi}_{0.5}\text{Mn}_{1.5}\text{O}_4$ in which Mn(IV) and a Ni(II) replace two Mn(III) are two promising cathode candidates for high-energy-density LIBs [11].

Lithium and manganese rich nickel-manganese-cobalt (LMR-NMC) oxides show higher charge/discharge capacity, typically $\geq 240 \text{ mAhg}^{-1}$ compared to stoichiometric nickel-manganese-cobalt (NMC)-type oxides (example: $\text{LiMn}_{1/3}\text{Ni}_{1/3}\text{Co}_{1/3}\text{O}_2$), LMR-NMC oxides suffer from voltage fade during electrochemical cycling, which renders them unsuitable for practical energy storage devices despite this high capacity. Voltage fading unfortunately continuously alters the cell capacity associated with a given state of charge (SOC). As a result it cannot satisfy constant power and energy requirements during operation. One of the major reasons for this voltage fade phenomenon has been attributed to a "layered to spinel (LS)" structural modification. However, the mechanism of this structural rearrangement is not fully understood.

Systematic ex-situ neutron diffraction on oxides was carried out on samples that were recovered at designated state of charges. The refined values of Li occupancy and location, modeling various possibilities of structure was used to uncover the transformation mechanisms in order to assist designing stable high-voltage oxides for high-energy-density Li-batteries. In this work it was shown that LS structural rearrangement in the LMR oxide occurs through a tetrahedral cation intermediate *via* the following two steps.

- i) First lithium atoms diffuses from octahedral to tetrahedral sites of the lithium layer [$\text{Li}_{\text{Li,oct}} \rightarrow \text{Li}_{\text{Li,tet}}$], which is followed by the distribution of the lithium ions from the adjacent octahedral site of the metal layer to the tetrahedral sites of the lithium layer [$\text{Li}_{\text{TM oct}} \rightarrow \text{Li}_{\text{Li,tet}}$];
- ii) Then a migration of Mn from the octahedral sites of the transition metal layer to the “permanent” octahedral site of the lithium layer takes place *via* the tetrahedral site of the lithium layer [$\text{Mn}_{\text{TMoct}} \rightarrow \text{Mn}_{\text{Li,tet}} \rightarrow \text{Mn}_{\text{Li,oct}}$].

Minimizing the spinel phase formation is one possible route to improve performance of these cathode materials. This can be accomplished by reducing the manganese content of LMR-NMC compounds would restrict the formation of Mn_{tet} , which is the major pathway to forming Mn_{Li} [12].

A series of work have also been carried out on high voltage spinel cathodes to study the role of cation ordering and surface segregation [13], integrated nano domains of ordered and disordered spinel phase [14].

4.2. SOLID ELECTROLYTES

An all solid-state battery is very attractive from a safety point of view, by avoiding flammable solvents and minimizing the possibility of a short circuit. Both a lack of solid electrolytes with acceptable ionic conductivity at room temperature, as well as difficulties with stability at the electrode-electrolyte interface, have hampered advances in this field [15]. One of the most promising candidates among the solid electrolytes is a Li-based garnet ceramic $\text{Li}_{7-x}\text{La}_3\text{Zr}_{2-x}\text{Ta}_x\text{O}_{12}$ that has a conductivity $\sigma_{\text{Li}} \sim 1.9 \times 10^{-3}$ S/cm at room temperature and is stable between 0 and 5.5 V vs Li/Li⁺ [16]. Because of its stability against metallic Li, and moderate stability in air, the cubic form of this compound has been at the forefront of current solid electrolyte research. The garnet framework is similar to the spinel framework in containing a tetrahedral A site bridged by octahedral sites. Each tetrahedral cubic 24d site is surrounded by four pairs of octahedrally coordinated 96h sites and all sites are partially occupied. In a series of detailed studies on these compounds using x-ray and neutron powder diffraction, electrochemistry and theoretical studies have shown that 0.4-0.5 Li vacancies per formula unit are required to stabilize the fast-ion conducting cubic garnet polymorph [17]. *Ex-situ* neutron diffraction played a critical role in correlating Li site occupancy with conductivity [18,19] to establish strategies to maximize performance.

5. CONCLUSION

When used in conjunction with property measurements neutron powder diffraction is a powerful tool to establish structure property relationships of materials used in electrochemical devices such as Li-ion batteries and solid oxide fuel cells. With concerns over the future availability of fossil fuels and climate change, scientists and engineers from all disciplines are focusing their research on materials for a sustainable future. The contribution of crystallography in reaching these goals has taken various forms and in this article I have highlighted how some of this work can help design alternate energy storage applications.

6. ACKNOWLEDGMENTS

This research at ORNL's Spallation Neutron Source was sponsored by the Scientific User Facilities Division, Office of Basic Energy Sciences, U.S. Department of Energy. The examples used here are all collaborative work with various different user groups at POWGEN instrument. All the original work is cited in the references.

7. REFERENCES

- [1] J.B. Goodenough, *Accounts of Chemical Research*. **46** (2011), 1053.
- [2] T.C. Hansen and H. Kohlmann, "*Z. Anorg. Allg. Chem.* **640** (2014), 3044.
- [3] B.C.H. Steele, *Solid State Ionics* **134** (2000), 3.
- [4] M.A. Tamimi and S. McIntosh, *Journal of Materials Chemistry A* **2** (2014), 6015.
- [5] R.A. Cox-Galhotra, A. Huq, J.P. Hodges, C. Yu, X. Wang, W. Gong, A. J. Jacobson and S. McIntosh, *Solid State Ionics* **249-250** (2013), 34.
- [6] R.A. Cox-Galhotra, A. Huq, J.P. Hodges, J. -H. Kim, C. Yu, X. Wang, A.J. Jacobson and S. McIntosh, *Journal of Materials Chemistry A* **1** (2013), 3091.
- [7] K. Mizushima, P.C. Jones, P.J. Wiseman and J.B. Goodenough, *Material Research Bulletin* **15** (1980), 783.
- [8] J.B. Goodenough, K. Mizushima and T. Takeda, *Journal of Applied Physics* **19** (1980), 305.
- [9] R. Yazami, P. Touzain, *Journal of Power Sources* **9** (1983), 365.
- [10] A. Yoshino, U.S. Patent No. 4, 688, 595 and JP No. 1989293, 1985.
- [11] J.B. Goodenough and K.S. Park, *Journal of the American Chemical Society* **135** (2013), 1167.
- [12] D. Mohanty, J. Li, D. P. Abraham, A. Huq, E. A. Payzant, D. L. Wood and C. Daniel, *Chemistry of Materials*, **26** (2014), 6272.
- [13] D. W. Shin, C. A. Bridges, A. Huq, M. P. Paranthaman and A. Manthiram, *Chemistry of Materials* **24** (2012), 3720.
- [14] J.H. Kim, A. Huq, M. Chi, N.P.W. Pieczonka, E. Lee, C.A. Bridges, M. Tessema, A. Manthiram, K.A. Persson and B.R. Powell, *Chemistry of Materials* **26** (2014), 4377.
- [15] J. Li, C. Ma, M. Chi, C. Liang and N. Dudney, *Advanced Energy Materials* **5** (2015), 1401408.
- [16] R. Murugan, V. Thangadurai and W. Weppner, *Angew. Chem. Int. Ed.* **46** (2007), 7778.
- [17] T. Thompson, J. Wolfenstine, J.L. Allen, M. Johannes, A. Huq, I.N. David and J. Sakamoto, *Journal of Materials Chemistry A* **2** (2014), 13431.
- [18] T. Thompson, A. Sharafi , A. Huq, J. L. Allen, J. Wolfenstine and J. Sakamoto, , *Advanced Energy Materials* **5** (2015), 1500096.
- [19] S. Mukhopadhyay, T. Thompson, J. Sakamoto, A. Huq, J. Wolfenstine, J. L. Allen, N. Bernstein, D. A. Stewart and M. D. Johannes, *Chemistry of Materials* **27** (2015), 3658.

MODIFICATIONS OF Mo_3Sb_7 VIA CHEMICAL SUBSTITUTION TO ENHANCE THE THERMOELECTRIC PROPERTIES

Quansheng Guo, Holger Kleinke

*Department of Chemistry and Waterloo Institute for Nanotechnology, Waterloo, ON, Canada
N2L 3G1*

Thermoelectric materials may convert waste heat into electricity, thereby contributing to a higher sustainability of today's society. Advanced thermoelectrics are heavily doped, narrow-gap semiconductors with heavy elements and complex crystal structures. As Mo_3Sb_7 is a metallic material, it needs to be modified via chemical substitution to obtain the missing valence electrons to become semiconducting. These modifications may take place either on the Mo or on the Sb sites, or by filling the cubic holes. Crystallography is an important tool to control and verify these substitutions, as well as to analyze the resulting changes. Here we report on our successful attempts to enhance the thermoelectric properties via Mo/Fe, Mo/Ni, and Sb/Te substitutions. In addition, the properties can be further modified via intercalations of Fe and Ni into these cubic holes, which often occur in competition with the substitutions on the Mo site.

1. INTRODUCTION

The thermoelectric energy generation may be used to a more sustainable energy usage of mankind, by utilizing waste heat, otherwise lost, to generate electricity, for example in automotives [1, 2]. Many researchers strive to increase its conversion efficiency, for it currently limits the applications of thermoelectrics. The efficiency increases with increasing thermoelectric figure-of-merit, namely $zT = T\alpha^2\sigma\kappa^{-1}$. Therein, α = Seebeck coefficient, σ = electrical conductivity, and κ = thermal conductivity. Typical thermoelectrics are properly doped semiconductors comprised of heavy elements, ideally with $zT > 1$ [3-7].

In 2002, we demonstrated that the metallic antimonide Mo_3Sb_7 turns into a *p*-doped semiconductor after partial Sb/Te exchange [8, 9]. Five years later, a zT of 0.76 at 1050 K was determined for $\text{Mo}_3\text{Sb}_{5.4}\text{Te}_{1.6}$ by Gascoin and Snyder et al. [10]. We further enhanced the figure-of-merit by intercalating Ni atoms into the voids of the Sb_8 cubes [11], culminating in $zT = 0.93$ for $\text{Ni}_{0.06}\text{Mo}_3\text{Sb}_{5.4}\text{Te}_{1.6}$, compared to 0.71 for $\text{Mo}_3\text{Sb}_{5.4}\text{Te}_{1.6}$ prepared and measured parallel in our group [12]. As tellurium is a rare and toxic element, it is desirable to find alternatives. One can also improve zT by partially replacing Mo with Fe [13, 14], Ni [15], or Ru [16, 17]. Here, we use crystallography to shine light on the different behavior of the Fe- and Ni-containing Mo_3Sb_7 variants.

2. EXPERIMENTAL SECTION

2.1 Synthesis and analysis

All reactions were carried out in fused silica tubes, starting from the elements as described earlier for the Fe variants [14]. Annealing temperatures of 873 K appeared to work best. We attempted to prepare phase pure samples of both $\text{Mo}_{3-x}\text{Fe}_x\text{Sb}_7$ and $\text{Mo}_{3-x}\text{Ni}_x\text{Sb}_7$ with $x = 0, 0.1,$

0.2, 0.3, 0.4, 0.45 and 0.5. First phase analyses were performed via powder X-ray diffraction using Inel's diffractometer with position-sensitive detector and Cu $K\alpha_1$ radiation. In case of Fe, the FeSb_2 peaks began to show when $x = 0.5$; in case of Ni, NiSb appeared already when $x = 0.3$ (and above). Thus we conclude that the phase width depends on the 3d metal, and that it is larger in case of Fe.

2.2 Single crystal studies

Single crystals were chosen from the samples of the nominal compositions $\text{Mo}_{2.55}\text{Fe}_{0.45}\text{Sb}_7$ and from $\text{Mo}_{2.8}\text{Ni}_{0.2}\text{Sb}_7$, i.e. at the end of the respective phase ranges. The data collections were performed at room temperature with a Bruker Kappa APEX II utilizing Mo $K\alpha$ radiation. Data were corrected for Lorentz and polarization effects, as well as for absorption using SADABS [18]. The refinements using the SHELXTL package [19] commenced from the published Mo_3Sb_7 data (space group $Im\bar{3}m$), where we allowed $M = \text{Fe}, \text{Ni}$ to substitute for Mo, while constraining the total occupancy of that metal site to 100%. In both cases, the R values were lowered after incorporating the 3d M atoms. In addition, we looked for the electron density at the center of the Sb_8 cubes, i.e. at the origin of the unit cell. There, we observed 0.5 electrons per \AA^3 in case of $M = \text{Fe}$, and 6.4 in case of $M = \text{Ni}$. A tentative refinement of that site with a partial occupancy of M resulted in 0% for Fe and 12% in case of Ni. The latter occurred with a significant improvement of $R1$ from 2.12% to 1.80%. The refined lattice parameters also point towards the existence of Ni in the cubes, as that is known to cause an enlargement of the unit cell [11]: $a = 9.5653(4)$ \AA for $\text{Ni}_{0.060(7)}\text{Mo}_{2.85}\text{Ni}_{0.15(9)}\text{Sb}_7$ is larger than $a = 9.559$ \AA typically measured for Mo_3Sb_7 , although the Mo/Ni substitution should shrink the unit cell, as Ni atoms are smaller than Mo atoms. On the other hand, $a = 9.5292(2)$ \AA for $\text{Mo}_{2.64}\text{Fe}_{0.36(5)}\text{Sb}_7$ is smaller than for Mo_3Sb_7 , in accord with the absence of Fe in the cubes and the Mo/Fe substitution causing a reduction in cell size. The respective atomic positions along with their occupancies are compared in Table 1.

TABLE 1.

Atomic positions and occupancy factors.

Atom	Wyckoff site	SOF (Fe)	SOF (Ni)
Mo1 \ M1 ^a	12e	0.879 \ 0.121(15)	0.95 \ 0.05(3)
Sb1 ^b	12d	1	1
Sb2 ^c	16f	1	1
M2 ^d	2a	0	0.120(14)

a) 12e: $x, 0, 0$ with $x = 0.3431(1)$ for $M = \text{Fe}$ and $0.3430(1)$ for $M = \text{Ni}$

b) 12d: $\frac{1}{4}, 0, \frac{1}{2}$

c) 16f: x, x, x with $x = 0.16224(4)$ for $M = \text{Fe}$ and $0.16254(4)$ for $M = \text{Ni}$

d) 2a: $0, 0, 0$

2.3 Physical property measurements

To prepare the materials for the measurements of the thermoelectric properties, the samples were thoroughly ground and then hot-pressed into round pellets of 12.7 mm diameter and 2 mm height in an argon atmosphere under a pressure of 46 MPa at 873 K for two hours, using Oxy-Gon FR-210-30T-ASA-160-EVC hot-press furnace system. Next, the thermal diffusivity, d , was determined from these pellets directly using the Anter (now TA Instruments) FlashLine™ 3000, also in an argon atmosphere. d was used to calculate the thermal conductivity, κ , via $\kappa = \rho C_p d$, with ρ the density of the pellet, and C_p the specific heat. C_p was taken from the Dulong-Petit law,

which works well for these materials [20]. Electrical conductivity and Seebeck coefficient were determined from a rectangular bar cut from the round pellets, using the ULVAC ZEM-3 in a helium atmosphere. Powder diffraction measurements after these property measurements showed no changes, i.e. the materials remained stable under the measurement conditions up to 800 K.

2.4 Electronic structure calculations

The calculations were based on density functional theory, using the WIEN2k package utilizing the full potential linearized augmented plane wave method (LAPW) [21] with the Perdew-Berke-Ernzerhof functional for the exchange correlation energy [22]. We calculated the density of states for Mo_3Sb_7 , and the models $\text{Mo}_{2.5}\text{Fe}_{0.5}\text{Sb}_7$, $\text{Mo}_{2.5}\text{Ni}_{0.5}\text{Sb}_7$, and $\text{Ni}_{0.25}\text{Mo}_{2.75}\text{Ni}_{0.25}\text{Sb}_7$. For the last three, one of the six Mo sites of the 1st Brillouin zone was replaced with an Fe or Ni atom (called Fe1 or Ni1), lowering the symmetry to space group $I4mm$. To model $\text{Ni}_{0.25}\text{Mo}_{2.75}\text{Ni}_{0.25}\text{Sb}_7$, an additional Ni atom (Ni2) was placed onto the origin (without any changes to the space group), i.e. into a cube formed by Sb atoms. Integrations in k space were performed on a $16 \times 16 \times 16$ mesh in each case.

3. RESULTS AND DISCUSSION

3.1 Crystal structure

Mo_3Sb_7 adopts the Ir_3Ge_7 structure type. Its structure is composed of square MoSb_8 antiprisms, which pairwise share a square face, resulting in an Mo–Mo bond of the order of 3.0 Å. These pairs are connected via intermediate Sb–Sb interactions of 3.1 Å to the next pair of antiprisms, which in the end leads to the formation of linear chains consisting of alternating antiprism pairs and empty cubes (Figure 1). The chains interpenetrate each other at these cubes, as each cube face is capped by an Mo atom. Furthermore, parallel running chains are interconnected via short Sb–Sb bonds of 2.9 Å.

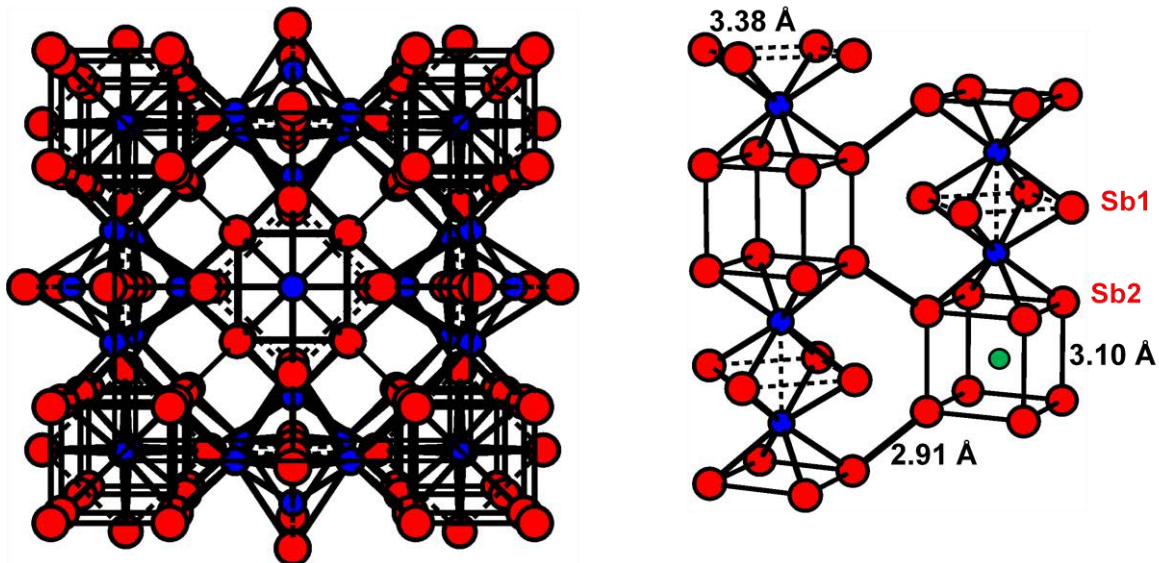


Figure 1. Left: Crystal structure of Mo_3Sb_7 ; right: section of the unit cell. Small, green circle: center of the Sb2 cube; medium, blue circles: Mo atoms; large, red: Sb.

Introducing the 3d elements Fe and Ni led to two different effects. In case of Fe, the Fe atoms were found to partially replace the Mo atoms in the square antiprisms, whereas in case of Ni, Ni atoms were found both in the Sb_8 square antiprisms as well as in the Sb_8 cubes. Hence, the nominal composition $Mo_{3-x}Fe_xSb_7$ appears to be correct, while " $Mo_{3-x}Ni_xSb_7$ " is more precisely written as $(Ni_2)_yMo_{3-x}(Ni_1)_xSb_7$, with Ni1 replacing Mo, and Ni2 occupying the centers of the Sb_8 cubes. The different behavior of Fe and Ni is likely related to i) steric effects and ii) Fe being more similar to Mo than Ni to Mo:

- i) The Slater radii for Fe and Ni are 1.40 Å and 1.35 Å, respectively. That even the smaller Ni atom barely fits into these cubes, reflects itself in an increase of the lattice parameter after the Ni addition. Therefore it is not surprising to observe at least a smaller tendency of Fe to fill the cubic void.
- ii) The larger similarity between Fe and Mo is based on size ($r_{Mo} = 1.45$ Å) as well as electronic effects, as for example Mo atoms have six valence electrons, compared to Fe's eight and Ni's ten.

3.2 Electronic properties

In order to gain insight into the different consequences of the different behavior of the Fe and Ni series, we computed the electronic structures of Mo_3Sb_7 as well as models with Fe and Ni replacing 1/6 of the Mo sites, called $Mo_{2.5}Fe_{0.5}Sb_7$, $Mo_{2.5}Ni_{0.5}Sb_7$. In addition, we used a model with the same Ni amount of 0.5 per formula unit, but half of that (Ni2) in the cubic voids, and half (Ni1) replacing Mo, resulting in the formula $Ni_{0.25}Mo_{2.75}Ni_{0.25}Sb_7$. This model then has a higher Mo amount compared to the other Ni-containing model, namely 2.75 vs. 2.5. The four densities of states are compared in Figure 2.

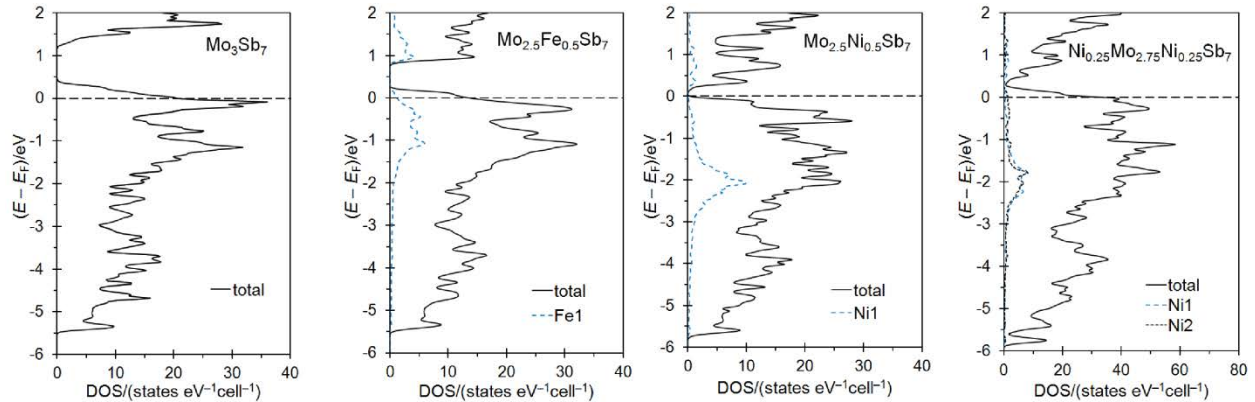


Figure 2. Density of states of Mo_3Sb_7 , $Mo_{2.5}Fe_{0.5}Sb_7$, $Mo_{2.5}Ni_{0.5}Sb_7$, and $Ni_{0.25}Mo_{2.75}Ni_{0.25}Sb_7$.

The parent compound, Mo_3Sb_7 , possesses a band gap located 0.5 eV above the Fermi level, corresponding to two unfilled bands per Brillouin zone, i.e. two Mo_3Sb_7 units. Thus, with Mo_3Sb_7 having $3 \times 6 + 7 \times 5 = 53$ valence electrons, the band gap would be reached with 55 valence electrons per formula unit, f. u.. Going from Mo_3Sb_7 to $Mo_{2.5}Fe_{0.5}Sb_7$, the valence electrons increase to 54 per f. u., thus the number of holes in the valence band decreases. In case of $Mo_{2.5}Ni_{0.5}Sb_7$ with 55 valence electrons, the Fermi level falls directly into the band gap. In addition, the size of the band gap shrinks by going from Mo_3Sb_7 to $Mo_{2.5}Fe_{0.5}Sb_7$ to $Mo_{2.5}Ni_{0.5}Sb_7$ (from left to right in Figure 2), and the features of the bottom of the conduction band change dramatically. Finally, the filled Fe states are closer to the band gap than those of Ni,

a consequence of the lower electronegativity of Fe compared to Ni.

The filling degree of the valence band of $\text{Ni}_{0.25}\text{Mo}_{2.75}\text{Ni}_{0.25}\text{Sb}_7$, on the other hand, closely resembles that of $\text{Mo}_{2.5}\text{Fe}_{0.5}\text{Sb}_7$, not that of $\text{Mo}_{2.5}\text{Ni}_{0.5}\text{Sb}_7$. The Ni2 atom in the Sb_8 cube does not alter the electron balance, as its ten valence electrons are used to fill its five 3d orbitals, all located in the valence band. Therefore, the valence band filling of $\text{Ni}_{0.25}\text{Mo}_{2.75}\text{Ni}_{0.25}\text{Sb}_7$ corresponds to that of $\text{Mo}_{2.75}\text{Ni}_{0.25}\text{Sb}_7$ (not shown here).

3.3 Physical properties

The properties of four samples are compared, with nominal compositions of Mo_3Sb_7 , $\text{Mo}_{3-x}\text{Fe}_x\text{Sb}_7$ with $x = 0.2$ and 0.45 , and $\text{Mo}_{3-x}\text{Ni}_x\text{Sb}_7$ with $x = 0.2$, labeled Mo_3Sb_7 , Fe0.2, Fe0.45, and Ni0.2 in the respective figures. It should be noted that the Ni0.2 sample (" $\text{Mo}_{2.8}\text{Ni}_{0.2}\text{Sb}_7$ ") actually contains Ni in the cubic holes as well as on the Mo sites, and thus an M : Sb ratio larger than 3 : 7, as reflected in the refined formula $\text{Ni}_{0.06}\text{Mo}_{2.85}\text{Ni}_{0.15}\text{Sb}_7$.

The electrical conductivity data are presented in Figure 3. Each material exhibits a relatively high conductivity, σ , around 300 K, ranging from approximately $4300 \Omega^{-1}\text{cm}^{-1}$ ($\text{Mo}_{2.55}\text{Fe}_{0.45}\text{Sb}_7$) to $6000 \Omega^{-1}\text{cm}^{-1}$ (Mo_3Sb_7), which decreases steadily with increasing temperature in every case, typical for materials with rather high carrier concentration. As predicted by the electronic structure calculations, adding these 3d elements causes a decrease of the carrier concentration, resulting in decreasing electrical conductivity with increasing 3d metal concentration. Since Ni atoms both occupy the cubic and the square antiprismatic sites, the Ni0.2 sample is predicted to have a similar carrier concentration as the Fe0.2 sample, and therefore a comparable electrical conductivity. These predictions are confirmed by the experiments:

$$\sigma(\text{Mo}_3\text{Sb}_7) > \sigma(\text{Mo}_{2.8}\text{Ni}_{0.2}\text{Sb}_7) \approx \sigma(\text{Mo}_{2.8}\text{Fe}_{0.2}\text{Sb}_7) > \sigma(\text{Mo}_{2.55}\text{Fe}_{0.45}\text{Sb}_7).$$

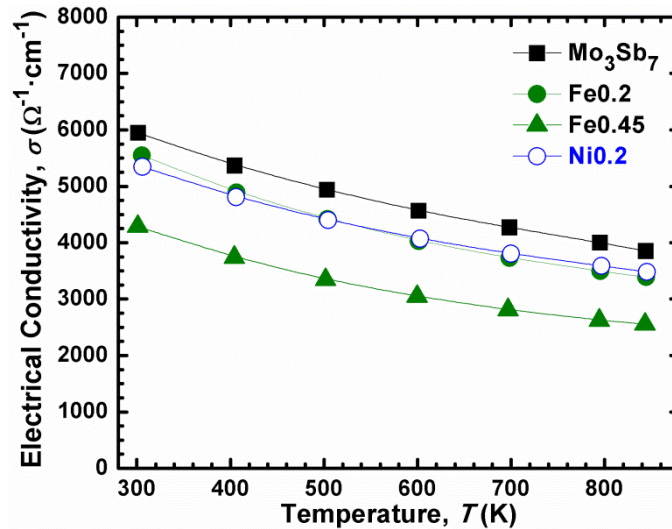


Figure 3. Electrical conductivity of Mo_3Sb_7 , $\text{Mo}_{2.8}\text{Fe}_{0.2}\text{Sb}_7$ (Fe0.2), $\text{Mo}_{2.55}\text{Fe}_{0.45}\text{Sb}_7$ (Fe0.45), and $\text{Mo}_{2.8}\text{Ni}_{0.2}\text{Sb}_7$ (Ni0.2). $\sigma(\text{Mo}_3\text{Sb}_7) > \sigma(\text{Mo}_{2.8}\text{Ni}_{0.2}\text{Sb}_7) \approx \sigma(\text{Mo}_{2.8}\text{Fe}_{0.2}\text{Sb}_7) > \sigma(\text{Mo}_{2.55}\text{Fe}_{0.45}\text{Sb}_7)$.

The Seebeck coefficient typically follows the opposite trend, i.e. it increases with decreasing carrier concentration (here: increasing 3d metal content). Again, the expectation, namely

$\alpha(\text{Mo}_3\text{Sb}_7) < \alpha(\text{Mo}_{2.8}\text{Ni}_{0.2}\text{Sb}_7) \approx \alpha(\text{Mo}_{2.8}\text{Fe}_{0.2}\text{Sb}_7) < \alpha(\text{Mo}_{2.55}\text{Fe}_{0.45}\text{Sb}_7)$, is experimentally confirmed, with $\alpha(\text{Mo}_{2.8}\text{Ni}_{0.2}\text{Sb}_7)$ being slightly smaller than $\alpha(\text{Mo}_{2.8}\text{Fe}_{0.2}\text{Sb}_7)$, as shown in Figure 4. Room temperature values range from $\alpha = +18 \mu\text{V K}^{-1}$ for Mo_3Sb_7 to $+31 \mu\text{V K}^{-1}$ for $\text{Mo}_{2.55}\text{Fe}_{0.45}\text{Sb}_7$, and are thus somewhat small for enhanced thermoelectrics, which often have $\alpha > 100 \mu\text{V K}^{-1}$. The positive sign of α points towards p -type charge carriers, in accord with a partially empty valence band as shown in Figure 2 for all models but $\text{Mo}_{2.5}\text{Ni}_{0.5}\text{Sb}_7$, which is beyond the experimentally observed phase range.

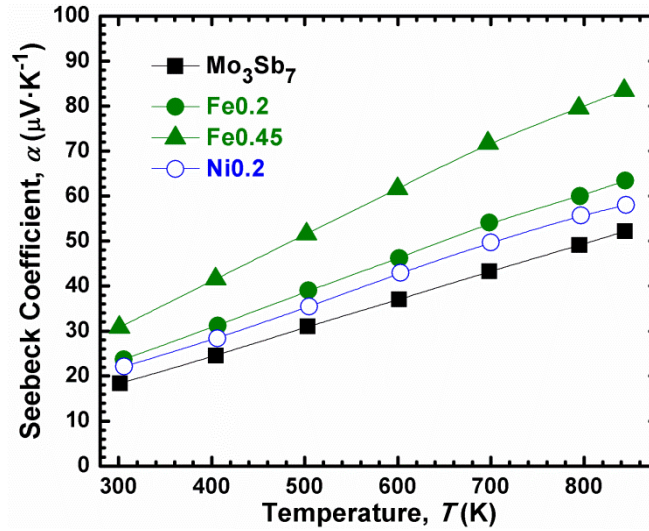


Figure 4. Seebeck coefficient of Mo_3Sb_7 , $\text{Mo}_{2.8}\text{Fe}_{0.2}\text{Sb}_7$ (Fe0.2), $\text{Mo}_{2.55}\text{Fe}_{0.45}\text{Sb}_7$ (Fe0.45), and $\text{Mo}_{2.8}\text{Ni}_{0.2}\text{Sb}_7$ (Ni0.2). $\alpha(\text{Mo}_3\text{Sb}_7) < \alpha(\text{Mo}_{2.8}\text{Ni}_{0.2}\text{Sb}_7) < \alpha(\text{Mo}_{2.8}\text{Fe}_{0.2}\text{Sb}_7) < \alpha(\text{Mo}_{2.55}\text{Fe}_{0.45}\text{Sb}_7)$.

The thermal conductivity, κ , corresponds to the sum of the electronic, κ_e , and lattice contributions, κ_L . κ_e is proportional to the product of the temperature and the electrical conductivity via $\kappa_e = L\sigma T$, with $L =$ Lorenz number. The rather high electrical conductivity causes the thermal conductivity values to be relatively high too, with values between $\kappa = 4.9 \text{ W m}^{-1}\text{K}^{-1}$ and $6.0 \text{ W m}^{-1}\text{K}^{-1}$ around 300 K (Figure 5). As the electrical conductivity appears as the dominating factor here, the order of these materials is the same in both thermal and electrical conductivity, i.e.:

$$\kappa(\text{Mo}_3\text{Sb}_7) > \kappa(\text{Mo}_{2.8}\text{Ni}_{0.2}\text{Sb}_7) \approx \kappa(\text{Mo}_{2.8}\text{Fe}_{0.2}\text{Sb}_7) > \kappa(\text{Mo}_{2.55}\text{Fe}_{0.45}\text{Sb}_7).$$

As demonstrated in Figure 6, the figure-of-merit, zT , increases with temperature as well as 3d element: $zT(\text{Mo}_3\text{Sb}_7) < zT(\text{Mo}_{2.8}\text{Ni}_{0.2}\text{Sb}_7) < zT(\text{Mo}_{2.8}\text{Fe}_{0.2}\text{Sb}_7) < zT(\text{Mo}_{2.55}\text{Fe}_{0.45}\text{Sb}_7)$. While an improvement from Mo_3Sb_7 to $\text{Mo}_{2.55}\text{Fe}_{0.45}\text{Sb}_7$ is evident, e.g. at 800 K from 0.11 to 0.29, we found $zT(800 \text{ K}) \approx 0.42$ for $\text{Mo}_3\text{Sb}_{5.4}\text{Te}_{1.6}$ and 0.50 for $\text{Ni}_{0.06}\text{Mo}_3\text{Sb}_{5.4}\text{Te}_{1.6}$ [12], and Candolphi et al. 0.45 for $\text{Mo}_{2.5}\text{Ru}_{0.5}\text{Sb}_{6.5}\text{Te}_{0.5}$ [23]. Since we were not able to incorporate more 3d elements into Mo_3Sb_7 , we conclude that the tellurium-free samples cannot easily match the performance of the Te-containing Mo_3Sb_7 variants.

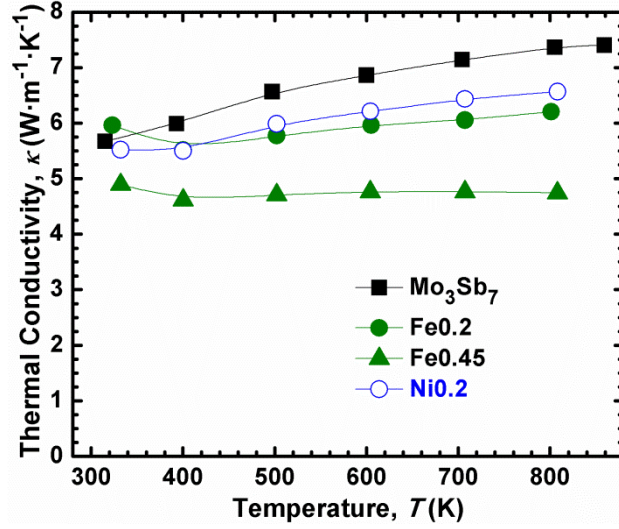


Figure 5. Thermal conductivity of Mo_3Sb_7 , $\text{Mo}_{2.8}\text{Fe}_{0.2}\text{Sb}_7$ (Fe0.2), $\text{Mo}_{2.55}\text{Fe}_{0.45}\text{Sb}_7$ (Fe0.45), and $\text{Mo}_{2.8}\text{Ni}_{0.2}\text{Sb}_7$ (Ni0.2). $\kappa(\text{Mo}_3\text{Sb}_7) > \kappa(\text{Mo}_{2.8}\text{Ni}_{0.2}\text{Sb}_7) \approx \kappa(\text{Mo}_{2.8}\text{Fe}_{0.2}\text{Sb}_7) > \kappa(\text{Mo}_{2.55}\text{Fe}_{0.45}\text{Sb}_7)$.

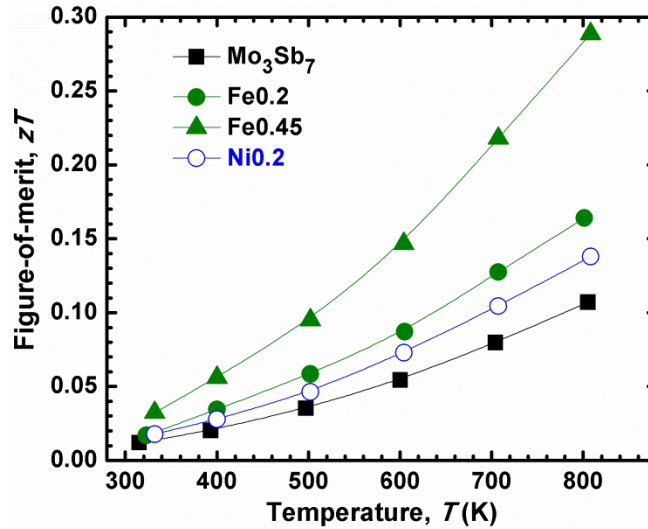


Figure 6. Figure-of-merit of Mo_3Sb_7 , $\text{Mo}_{2.8}\text{Fe}_{0.2}\text{Sb}_7$ (Fe0.2), $\text{Mo}_{2.55}\text{Fe}_{0.45}\text{Sb}_7$ (Fe0.45), and $\text{Mo}_{2.8}\text{Ni}_{0.2}\text{Sb}_7$ (Ni0.2). $zT(\text{Mo}_3\text{Sb}_7) < zT(\text{Mo}_{2.8}\text{Ni}_{0.2}\text{Sb}_7) < zT(\text{Mo}_{2.8}\text{Fe}_{0.2}\text{Sb}_7) < zT(\text{Mo}_{2.55}\text{Fe}_{0.45}\text{Sb}_7)$.

4. CONCLUSIONS

The thermoelectric properties of Mo_3Sb_7 can be enhanced via incorporation of the 3d metals Fe and Ni. While the Fe atoms exclusively substitute for the Mo atoms, the Ni atoms additionally occupy cubic voids formed by the Sb atoms. When these 3d elements occupy the Mo sites, their valence electrons fill some of the holes in the valence band of Mo_3Sb_7 . This is in contrast to the Ni atoms in the cubic voids, which do not fill these holes, as they also add bands to the valence band.

Up to 0.45 Fe atoms and 0.2 Ni atoms, respectively, can be incorporated into Mo_3Sb_7 . The samples with 0.2 Fe and 0.2 Ni are very comparable in their thermoelectric properties, while the

one with 0.45 Fe is the best of these series. Still, its performance is not comparable to the Te-substituted variants, most notably Ni_{0.06}Mo₃Sb_{5.4}Te_{1.6}.

ACKNOWLEDGMENTS

Financial support from the Natural Sciences and Engineering Research Council is appreciated.

REFERENCES

- [1] L.E. Bell, *Science* **321** (2008), 1457.
- [2] J. Yang and F.R. Stabler, *J. Electron. Mater.* **38** (2009), 1245.
- [3] D.M. Rowe, *Thermoelectrics Handbook: Macro to Nano*. (CRC Press, Taylor & Francis Group, Boca Raton, FL, USA, 2006).
- [4] H. Kleinke, *Chem. Mater.* **22** (2010), 604.
- [5] E.S. Toberer, A.F. May and G.J. Snyder, *Chem. Mater.* **22** (2010), 624.
- [6] M.G. Kanatzidis, *Chem. Mater.* **22** (2010), 648.
- [7] Q. Guo, A. Assoud and H. Kleinke, *Adv. Energy Mater.* **4** (2014), 1400348.
- [8] E. Dashjav, A. Szczepienowska and H. Kleinke, *J. Mater. Chem.* **12** (2002), 345.
- [9] J. Xu and H. Kleinke, *J. Comput. Chem.* **29** (2008), 2134.
- [10] F. Gascoin, J. Rasmussen and G.J. Snyder, *J. Alloys Compd.* **427** (2007), 324.
- [11] N. Soheilnia, E. Dashjav and H. Kleinke, *Can. J. Chem.* **81** (2003), 1157.
- [12] H. Xu, K.M. Kleinke, T. Holgate, H. Zhang, Z. Su, T.M. Tritt and H. Kleinke, *J. Appl. Phys.* **105** (2009), 053703.
- [13] C. Candolfi, B. Lenoir, A. Dauscher, B. Malaman, E. Guilmeau, J. Hejtmánek and J. Tobola, *Appl. Phys. Lett.* **96** (2010), 262103.
- [14] Q. Guo and H. Kleinke, *J. Solid State. Chem.* **215** (2014), 253.
- [15] X. Deng, M. Lü and J. Meng, *J. Alloys Compd.* **577** (2013), 183.
- [16] C. Candolfi, B. Lenoir, J. Leszczynski, A. Dauscher, J. Tobola, S.J. Clarke and R.I. Smith, *Inorg. Chem.* **48** (2009), 5216.
- [17] C. Candolfi, B. Lenoir, J. Leszczynski, A. Dauscher and E. Guilmeau, *J. Appl. Phys.* **105** (2009), 083701.
- [18] *M86-Exx078 APEX2 User Manual*. (Bruker AXS Inc., Madison, WI, 2006).
- [19] G.M. Sheldrick, *Acta Crystallogr. A* **64** (2008), 112.
- [20] N. Nandihalli, A. Lahwal, D. Thompson, T.C. Holgate, T.M. Tritt, V. Dassylva-Raymond, L.I. Kiss, E. Sellier, S. Gorsse and H. Kleinke, *J. Solid State Chem.* **203** (2013), 25.
- [21] P. Blaha, K. Schwarz, G.K.H. Madsen, D. Kvasnicka and J. Luitz, *WIEN2k, An Augmented Plane Wave + Local Orbitals Program for Calculating Crystal Properties*. (Techn. Universität Wien, Austria, 2001).
- [22] J.P. Perdew, K. Burke and M. Ernzerhof, *Phys. Rev. Lett.* **77** (1996), 3865.
- [23] C. Candolfi, B. Lenoir, A. Dauscher, E. Guilmeau and J. Hejtmánek, *J. Appl. Phys.* **107** (2010), 093709.

ELUCIDATING THE STRUCTURE OF IONIC LIQUIDS BY X-RAY DIFFRACTION NEW OPPORTUNITIES FOR MATERIALS DESIGN

Anja-Verena Mudring

*Dept. of Materials Science and Engineering, Iowa State University, Ames, IA 50011, USA
The Critical Materials Institute, Ames Laboratory, U.S. Department of Energy, Ames, IA 50011,
USA*

ABSTRACT

Ionic liquids (ILs), salts with a melting point lower than 100°C – many of them are room temperature ionic liquids (RTILs) – have received a tremendous interest both in academia and industry over the past two decades that seems not to stop. Because of their often low vapor pressure and inflammability ILs are frequently discussed in the context of green chemistry. However, ILs are not green *per se* – but they can be made green and a number of applications are now established that meet the criteria for a green(er) process. Currently it is realized that their modular character allows to engineering an IL for a certain application. Yet predictions which ion combinations to choose that give rise to a RTIL with the desired properties are difficult. Analysis of their complex structural behavior by means of X-ray structure analysis is challenging but allows for important insights. Since RTILs are liquid at room temperature it is not an easy task to crystallize them for X-ray structure analysis. We will discuss crystallization techniques for ILs and discuss an example where X-ray structure analysis of a set of ILs allows to gain valuable insights into property-relationships in ionic liquids and helps to formulate design principles for RTILs. On the whole, this contribution intends to give insights into the liquid-solid phase transition of ionic liquids from the viewpoint of crystallography and hopes to contribute to a better understanding of this intriguing and exciting class of compounds.

1. INTRODUCTION – WHY STUDY THE STRUCTURE OF IONIC LIQUIDS?

Ionic liquids (ILs), salts with a melting point lower than 100°C have received a tremendous interest both in academia and industry over the past two decades that seems not to stop. Many of these unique low melting salts solidify even below room temperature (RTILs, room temperature ionic liquids). It is their unusual and unique properties and property combinations that renders them so interesting for a great number of applications. ILs are not necessarily new materials, examples have been known for over 100 years, [1] but have gained renewed interest over the last 20 years, and particularly from 1995 onwards, first due to efforts by the United States Air Force in applying ILs as electrolytes, and then as a result of suggestions that ILs have unique properties as replacements of conventional solvents.[2] Because of their often low vapor pressure and inflammability they are frequently discussed in the context of green chemistry.[3] However, it turned out that ILs are not green *per se* – but they can be made green, and a number of chemical processes are now established that meet the criteria of green chemistry.[4]

What is intriguing from a fundamental point of view, is that it is possible to carry out chemistry in a truly ionic medium, something that is not possible in conventional molecular solvents and in classical molten salts, since their melting points are well beyond the degradation temperatures of organic compounds. Here it was soon realized that the IL itself can control the outcome of a chemical reaction. It is possible to control the phase for a polymorphic material by the IL [5], it is

also possible to control the size and morphology of nanomaterials [6]. Materials that are inaccessible from conventional solvents can be made in these ionic media [7] and, as a final point, the IL can control the product selectivity in organic reactions.[8] Thus, the solvent is no longer an innocent spectator, but it critically steers the product formation. Since an IL is composed of a cation and an anion, its properties are determined by the single ions as well as their combination. Thus, ILs offer the unique possibility to design and engineer a solvent and reaction medium for a given application through deliberate ion variation.

The intense scrutiny that ILs have received has led to an explosion in the number of new ion classes known to support IL behavior (a sample is provided in Fig. 1). These stretch from the well-recognized azolium (e.g., imidazolium, triazolium) over phosphonium, pyridinium, pyrrolidinium, alkylammonium etc. cations, to many new cation classes. Anions include both a wide variety of inorganic anions (e.g., halide, nitrate, perchlorate, sulfate, nitrite, hexafluorophosphate, tetrafluoroborate, azide) and an ever increasing number of organic anions (e.g., triflate, benzoate, sulfacetamide, alkylsulfates, alkylcarbonates, carboxylates).[9]

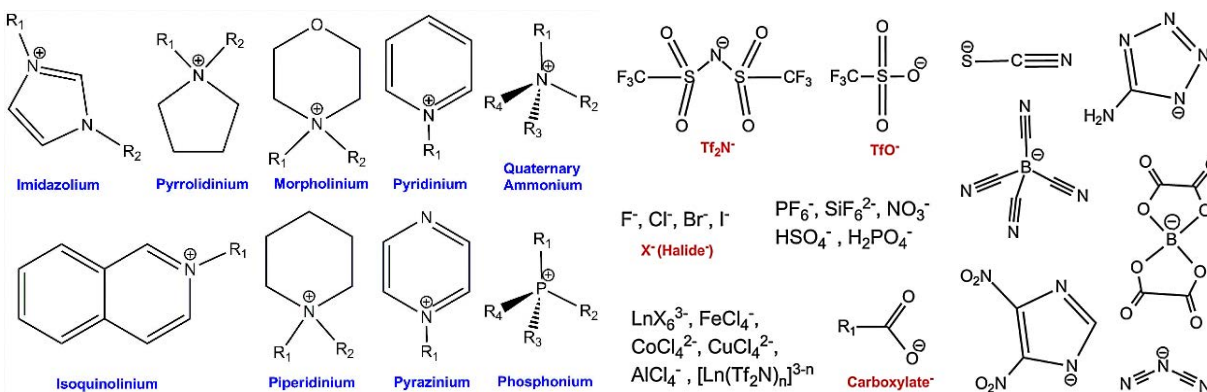


Figure 1. A few known IL forming ions.

A number of further questions are still inadequately answered: Why have certain ionic liquid compounds such a low melting point? How to design a cation-anion combination that results in a room temperature or below solidifying salt? Which factors favor a low melting point? What kind of specific interactions have to be avoided? What interactions occur in low melting salts that may favor a low melting point? The approach to design the IL's cation and anion combination in such a way that crystallization is suppressed has been coined "anti-crystal engineering" [10]. In this respect X-ray structure analysis can lead to a deeper understanding. It can be imagined that crystallization of ILs is not easy to achieve. ILs tend to supercool drastically and often rather form glasses upon cooling than crystalline material. A number of ILs feature the formation of mesophases like liquid crystals or plastic crystals before crystallization. Even in the crystalline state complex solid-solid phase transitions can occur. Thus, analysis of their complex structural behavior is challenging but allows for fundamental insights and, in the end, will help to find guidelines for optimal ionic liquid design.

2. AMMONIUM-BASED IONIC LIQUIDS AS AN EXAMPLE

A recent example where "anti-crystal engineering" is important is the application of pharmaceutically active ionic liquids.[11] Conventional drugs, which are composed of ions, are

commonly applied as sodium or halide salts, which are usually solid at room temperature. Their solubility certainly affects their bioavailability and their pharmacokinetical efficiency which quite often is determined by their solubility. One possibility to overcome this problem is to combine pharmaceutically active ions with counterions with the ion combination giving rise to a room temperature ionic liquid.

Many, sometimes quite simple, ammonium salts such as ammonium chloride (an expectorant) [12] or choline salts (common anti-inflammatory drugs) [13] are used for conventional drugs. For that reason, studying the solidification behavior and solid state structures of simple ammonium cations with various anions is interesting. An exemplary set of ion combinations that were studied by us is shown in Figure 2. Salts with trimethyl-N-3-hydroxypropylammonium or 3-hydroxypropylammonium as the cation and formate or bis(trifluoromethanesulfonyl)amide were synthesized and their crystallization properties studied. Both the cations and anions have different size and packing requirements and, most importantly, different capacities for secondary bonding such as hydrogen bonding.

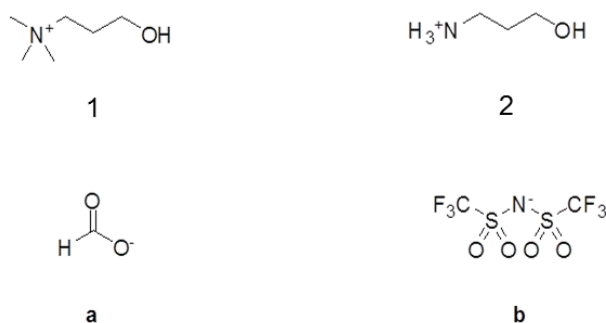


Figure 2. Ion combinations under investigation.

Differential scanning calorimetry (DSC) reveals different thermal behavior for the four compounds under investigation, see Figure 3. Trimethyl-2-hydroxypropylammonium formate (**1a**) melts upon heating at 99.2°C and crystallizes at 56.2°C upon cooling. Strong supercooling is commonly observed for ionic liquids and illustrates how important the kinetics of phase transformation are for this class of compounds. The enthalpy of melting was determined to 26 kJ/mol and was fully recovered upon cooling. In contrast, with the bis(trifluoromethanesulfonyl)amide anion (**b**) a compound forms that shows only a glass transition (**1b**) around -70°C. From that, one could anticipate that formate (**a**) is promoting the crystallization, maybe through its smaller size and hydrogen bonding capabilities, and the larger bis(trifluoromethanesulfonyl)amide (**b**) hampers crystallization. The latter anion is more hydrophobic and less apt to engage in hydrogen bonding, the rotation barriers around the N-S and S-C bonds are quite low giving rise to high structural flexibility at low temperatures and below. However, when pairing the formate anion (**a**) with the primary ammonium cation 3-hydroxypropylammonium, a thermal behavior similar to that of **1b** is observed for compound **2a**. The glass transition occurs at slightly lower temperatures (-83°C) and is fully reversible. NMR spectroscopy shows that at room temperature 3-hydroxypropylamine and formic acid are in equilibrium with **2a** which probably prevents crystallization. Bis(trifluorosulfonyl)amine is a much stronger acid than formic acid, for that reason such an equilibrium cannot be observed for 3-hydroxypropylammonium bis(trifluoromethane)sulfonylamide (**2b**). This compound features a thermal behavior quite often observed for ionic liquids. Once molten, upon cooling the material does not crystallize but rather solidifies as a glass.

However, upon heating cold-crystallization at -13°C is observed before the compound melts at $+13^{\circ}\text{C}$.

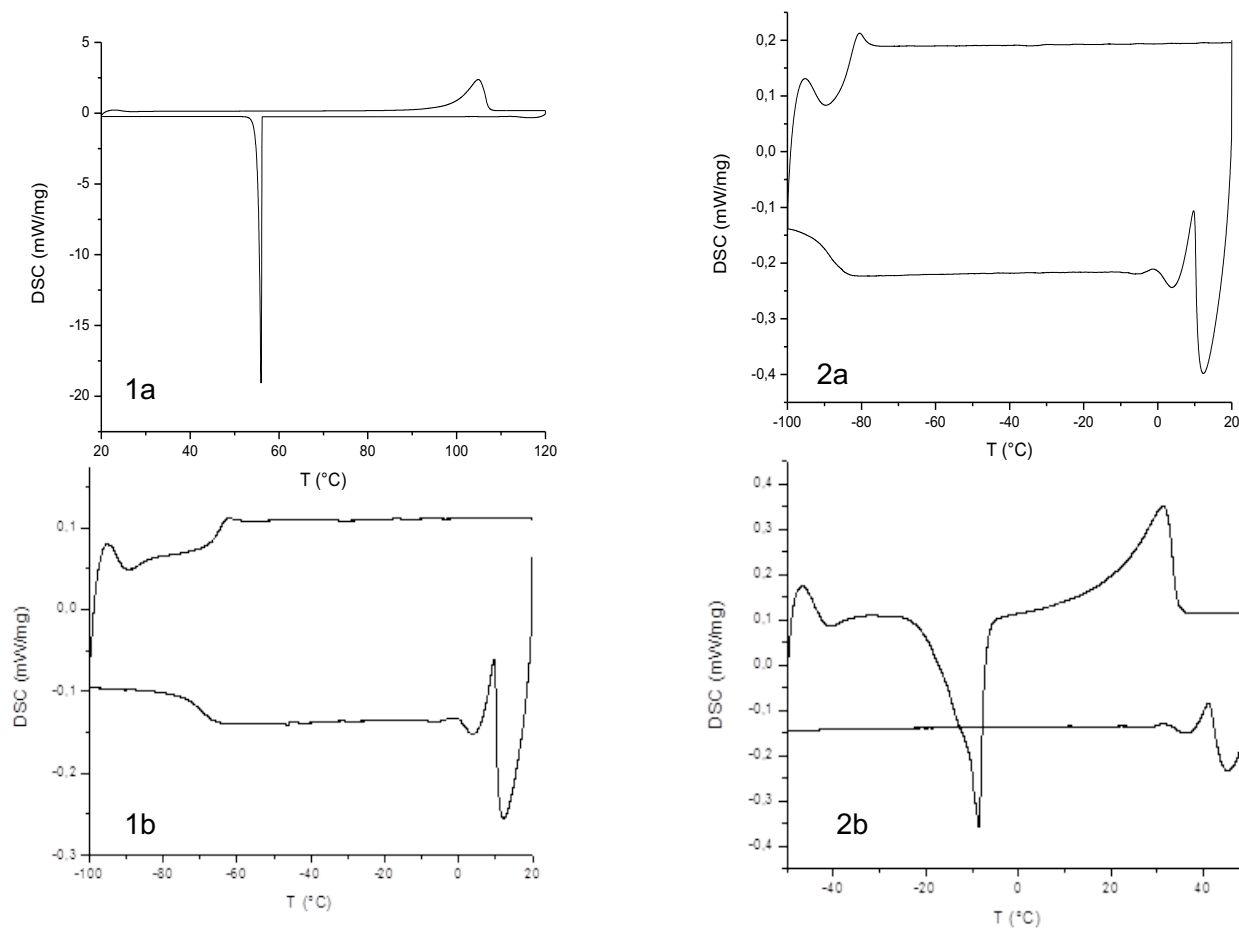


Figure 3. DSC traces (heating top line, cooling bottom line, endothermal events up, thermal ramp $10^{\circ}\text{C}/\text{min}$) for compounds under investigation.

The question now is how to obtain good crystals of compounds that feature this kind of thermal behavior. More specifically, crystals of a material that does not crystallize upon cooling, but upon heating, yet below ambient temperature, and then even melts below room temperature. For this special crystallization techniques are needed.

3. CRYSTALLIZATION TECHNIQUES FOR IONIC LIQUIDS

In order to be able to study the crystal structure of RTILs single crystals need to be grown of a quality high enough for X-ray structure analysis. Here, in principle, two basic approaches are possible –growth of single crystals from the melt or from solution, both at low temperatures. From a thermodynamic viewpoint crystallization has to occur when the Gibbs free energy of the solid is less than that of the melt. Then the decrease in entropy due to ordering of the ions upon

crystallization is overcompensated by the release of enthalpy. On a microscopic level, crystallization occurs stepwise and can be divided into nucleation and crystal growth.

Already Tammann has studied extensively the nucleation behavior of organic melts and observed that the temperature of the maximum rate of nucleation can be considerably below the temperature of the maximum rate of crystal growth leading to supercooling.[14] Indeed, many ionic liquids show this phenomenon and supercooling of 50°C at heating rates of 5°C/min are not uncommon.[15] Larger thermal ramps will lead to even higher deviations of crystallization peaks and melting points. Even worse, crystallization is hampered in many ionic liquids to such a degree that even upon moderate cooling rates they will solidify as a glass. The higher the cooling rate the less time is available to sample configurations at a given time and the earlier deviation from the thermodynamic equilibrium occurs and eventually glass formation sets in. For that reason special techniques for the crystallization from the melt are needed.

A technique that has been proven to be an extremely powerful tool to grow crystals of sub-ambient melting compounds on the diffractometer is in situ cryo-crystallization.[16] For the crystal growth of RTILs on the diffractometer, the IL is first introduced under an inert gas atmosphere into a Lindemann glass capillary (preferably 2.5 cm long and 0.3 mm in diameter), sealed and mounted on the diffractometer in a cooling gas stream. Subsequently the ionic liquid is carefully subjected to repeated cooling and warming until it no longer is a glass but a polycrystalline material. At this point a modified zone-melting technique is used to grow a single crystal of good quality by heating a small section. About ~1 mm of the lower portion of the capillary is heated by an IR laser to create a zone of molten material which is then slowly moved up along the capillary while the laser power is adjusted to sufficiently melt the polycrystalline material. The laser beam is moved along the whole capillary from bottom to top in approximately one hour. The laser power is then slowly reduced and the cycles repeated several times until a single crystal of sufficient quality for data acquisition has been grown.

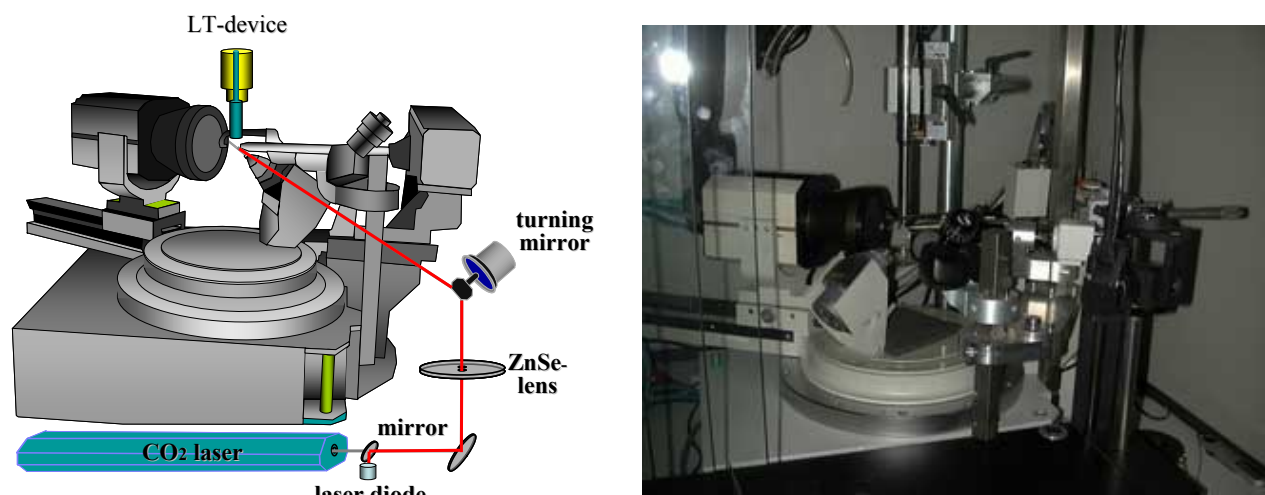


Figure 4. Optical heating and crystallization device (OHCD).[17]

By far the most common route to crystallize ionic liquids is from solution in volatile organic solvents. The advantage of this method is the higher ion mobility, but sometimes it is not easy to find the right solvent and solvent combination that allows for the optimum growth conditions of

single crystals. Methanol [18], acetonitrile [19], ethylacetate [20], dichloromethane [21] and diethylether/acetonitrile solvent mixtures [22] are the most common crystallization solvents for ionic liquids, but even water [23] has been used successfully. Yet it has to be kept in mind that using water often yields hydrates, especially in the case of halide anions.[24] As well, even apolar organic solvents such as benzene can get incorporated when the IL is hydrophobic. [25] In all cases where crystals are grown from solution one has to be very careful that no solvent is included in the final crystallization product. A good starting concentration of the IL in the solvent for crystallization is about 5-30 wt%. The volatile solvent is then evaporated from the solution, either under reduced pressure and/or at elevated temperatures. If this does not yield crystals of sufficient quality for structure analysis, slower removal of the solvent is required. This may be achieved by slow isothermal evaporation of the solvent, which is feasible even at low temperatures. The solvent has not to be removed completely, the crystals can be separated from the mother liquor.

However, if the IL features a melting point below room temperature special techniques for crystal selection and mounting have to be used. Crystals grown by this procedure can be best selected at low temperatures and mounted on the diffractometer using a modification of the oil-drop method initially described by Kottke and Stalke.[26] The mother liquid containing the crystals is transferred with a spoon (Figure 5, d) from the crystallization container onto a glass plate (a) which is cooled by a liquid nitrogen bath (b) or dry ice/ethanol from below. Nitrogen gas is blown through a copper spiral (c) that is immersed in liquid nitrogen (b) above the sample. The temperature of the gaseous nitrogen can be adjusted by the speed of the nitrogen stream. To prevent hydrolysis or oxidation of air-sensitive compounds the sample might be coated with a perfluorinated polyether. In the case of an ionic liquid, the IL itself seals often sufficiently from the atmosphere. After separating the crystals with a glass needle (e), the desired crystal can be directly transferred to the goniometer head (f). Most conveniently the goniometer head tip is equipped with a flexible nylon loop of appropriate diameter so that capillary forces hold the crystal in the middle of this loop.[27] The goniometer head tip is immersed in liquid nitrogen and transferred to the diffractometer for quality check and data collection.

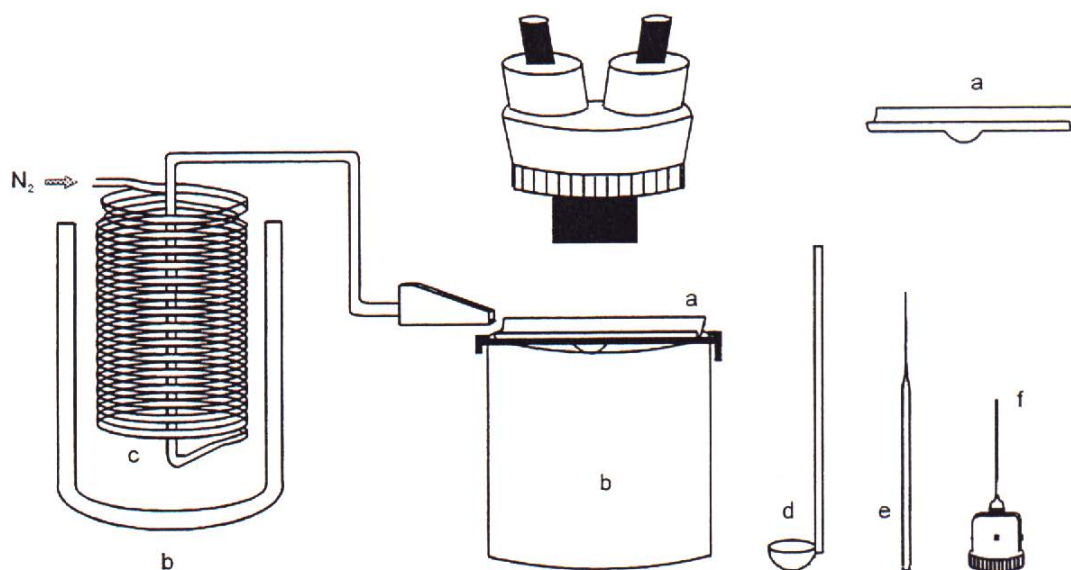


Figure 5. Crystal selection and mounting at low temperatures.

4. IONIC LIQUID CRYSTAL STRUCTURES AND WHAT DO WE LEARN FROM THEM

Crystals of trimethylammonium-3-hydroxypropyl formate (**1a**) could be successfully grown from solution while for compound **2b**, 3-hydroxymethylammonium bis(trifluoromethanesulfonyl)amide, only in-situ crystallization on the diffractometer yielded crystals that allowed for single X-ray structure analysis.

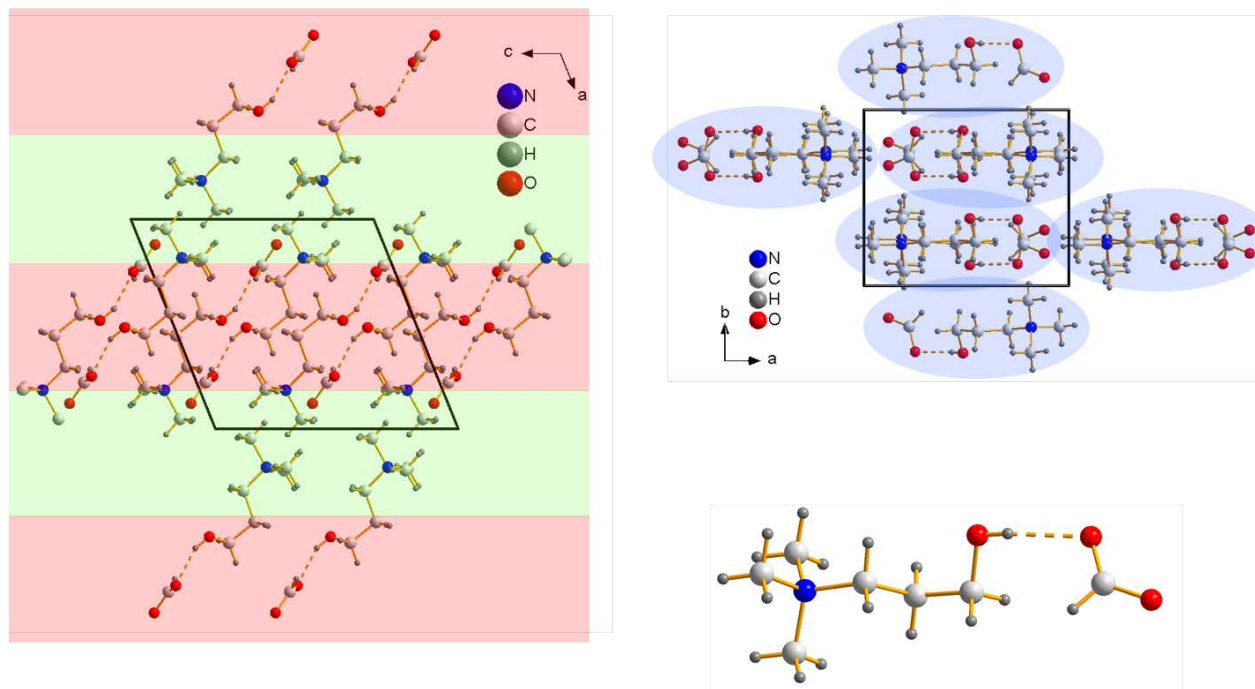


Figure 6. Left and top right: Projections of the crystal structure of **1a**. Bottom right: Trimethylhydroxypropyl formate ion pair, hydrogen bonds indicated by fragmented lines.

Examining the crystal structure of trimethylammonium-3-hydroxypropylammonium formate (**1a**) intriguingly reveals hydrogen bonded trimethylammonium-3-hydroxypropylammonium-formate ion pairs (Fig. 6, bottom right). The crystal structure of **1b** is built up by an assembly of these ion pairs as shown in Fig. 6, top right, where the ion pairs are encircled in blue. They assemble in such a way that layers in which hydrogen bonding between the hydroxyl group of the cation and one oxygen atom of the formate anion (shown in red in Fig. 6, left) prevail are separated by layers in which van der Waals interactions between the trimethylammonium headgroups of the cation predominate (shown in green in Fig. 6, left). Astonishingly, the shortest contacts are not between the formate anion and the charged trimethylammonium headgroup of the cation. Apparently additional energy to the mere electrostatic interaction can be gained by secondary bonding, namely hydrogen bonding and van der Waals bonding.

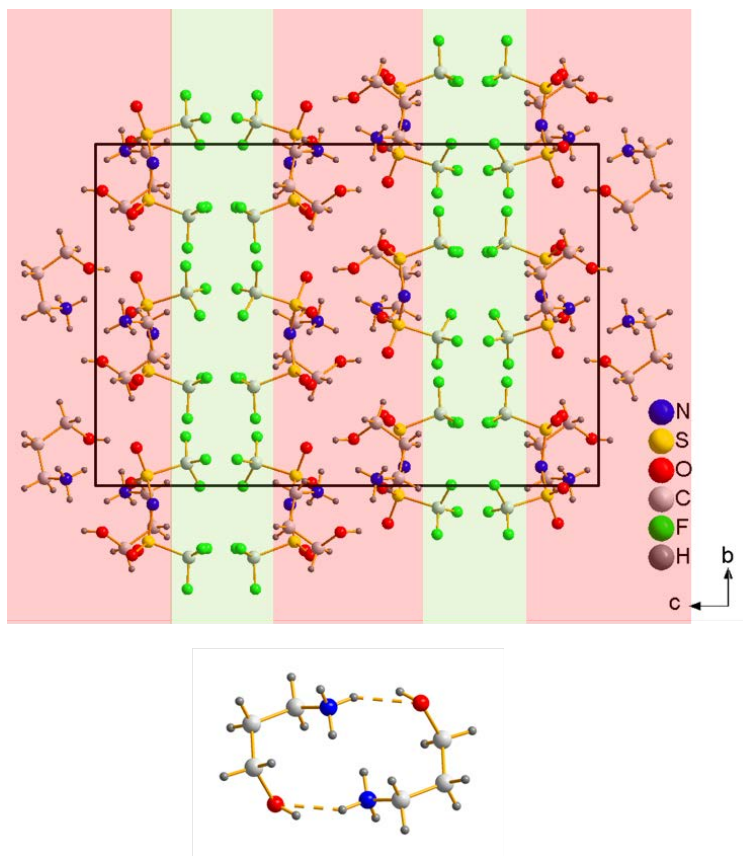


Figure 7. Top: projection of the crystal structure of **2b**. Bottom: 3-Hydroxymethylammonium ion pair, hydrogen bonds indicated by fragmented lines.

Looking at the crystal structure of 3-hydroxypropylammonium bis(trifluoromethanesulfonyl)amide (**2b**) a similar segregation into different structural domains can be observed (Fig. 7). Most evident are areas, shaded in green in Fig. 7 top, where halogen bonding prevails. This area is made up by double layers of bis(trifluoromethanesulfonyl)amide anions in the *cis* conformation. Albeit the *trans* conformation is the energetically preferred conformation in the gas phase [28], adopting the *cis* conformation allows for forming a layered structure where halogen-halogen interactions become possible. These areas are separated by charged regions which are made up by the charge-bearing sulfonylamide units of the anion and the 3-hydroxypropylammonium cation. Inspecting the cation's environment more closely reveals that two cations form a hydrogen bonded dimer (Fig. 7, bottom). So, again, secondary bonding determines that structural arrangement of cation and anions in the solid.

5. CONCLUSIONS AND SUMMARY

To summarize the observations: Four compounds made up of ion combinations of trimethyl-3-hydroxypropylammonium (**1**) and 3-hydroxypropylammonium (**2**) as the cations and formate (**a**) and bis(trifluoromethanesulfonyl)amide (**b**) as the anions were synthesized and their thermal behavior with respect to the formation of an ionic liquid investigated. Formally all compounds qualify as ionic liquids with melting points or glass transitions to occur below 100°C. Yet, on a second look, for all compounds distinctly different thermal behavior was observed. The combination of the trimethyl-3-hydroxypropylammonium cation (**1**) with the formate anion (**b**)

gave rise to a salt with a melting point close to 100°C. The compound crystallized easily. Crystal structure analysis reveals as the main structural feature cation-anion pairs with strong directional hydrogen bonds. They are assembled to the 3D structure by optimizing van der Waals interactions. Pairing the same cation (trimethylammonium-3-hydroxypropylammonium, **1**) with the bis(trifluoromethanesulfonyl)amide anion (**b**) yielded a salt for which only glass transitions could be observed. All attempts for crystallization failed. This is attributed to the fact that the anion is an extremely weak base and is unlikely to engage in directional hydrogen bonds. In addition the anionic charge is well spread over the entire, low symmetry anion which makes the formation of directional interactions difficult. Crystallization may be further hampered by the shallow energy barrier between the *transoid* and *cisoid* conformations of the anion which additionally inhibit assembly to a well-ordered structure by structural frustration. However, when combining the bis(trifluoromethanesulfonyl)amide anion (**b**) with a cation that has higher potential for hydrogen bonding, *i.e.*, the 3-hydroxypropylammonium cation (**2**) it becomes possible to crystallize this salt through careful heat treatment. Crystallization from the liquid is still hampered and upon cooling a glass forms. One reason for this observation may be the structural flexibility of the anion even at lower temperatures, another reason may lie in hydrogen-bonding frustration. However, careful heat treatment of the ionic liquid makes it possible to crystallize the material. Inspection of the crystal structure reveals, aside from fluorine-fluorine interactions, strong hydrogen bonding between cation pairs. It can be imagined that, once molten, hydrogen bonding frustration amongst the cations exist which make it difficult for the material to crystallize at moderate cooling rates. This assumption is further supported by the thermal behavior of 3-hydroxypropylammonium formate (**2a**). Here both the cation and the anion have a high capability to engage in hydrogen bonding. In addition 3-hydroxypropylamine and formic acid are both a comparatively weak base and acid so that an equilibrium between free base and acid and the salt is observed which relies on proton exchange. This leads to critical hydrogen bonding frustration and ultimately prohibits crystallization.

6. OUTLOOK

Solidification and especially crystallization of ionic liquids is by no means an easy task. It becomes technically more demanding the lower the melting point of the respective ionic liquid is. With the vast number of ionic liquids that have been described to date, only a small number of these compounds have been crystallized and structurally studied in the solid state. However, we may get important information on the interactions and with that be able to modify ionic liquids to suppress the melting point even more by “anti-crystal engineering”. Looking at the enormous diversity of solid phases that may form ionic liquids – well-ordered and disordered crystals, plastic crystals and different liquid crystalline phases – the study of the solid state of ionic liquids will prove existing theories and help to drive research further in this area.

ACKNOWLEDGEMENT

This work has been supported by Iowa State University and the Ames Laboratory, U.S. Department of Energy.

REFERENCES

- [1] B. Chan, N. Chang, M. Grimmer, *Austr. J. Chem.* **1977**, *30* (9), 2005-2013; S. Sugden, H. Wilkins, *J. Chem. Soc.*, **1929**, 1291-1298; P. Walden, *Bull. Acad. Imper. Sci. (St. Petersburg)*, **1914**, *8*, 405-422; O. Wallach, *Ber. dt. Chem. Ges.* **1882**, *15*, 644-652.
- [2] Y. Chauvin, H. Olivierbourbigou, *Chemtech*, **1995**, *25*, 26-30; C.L. Hussey, *Pure Appl. Chem.*, **1988**, *60* (12), 1763-1772; K.R. Seddon, In *Molten Salt Forum*, Proceedings of the 5th International Conference on Molten Salt Chemistry and Technology, pp. 53-62, **1998**; J.S. Wilkes, J.A. Levisky, R.A. Wilson, C.L. Hussey, *Inorg. Chem.* **1982**, *21*, 1263-1264.
- [3] R.D. Rogers, K.R. Seddon (Eds.), *Ionic Liquids as Green Solvents – Progress and Prospects*, ACS Symposium Ser. 2003, American Chemical Society.
- [4] H. Saitoh, Introduction of BASILTM (Biphasic Acid Scavenging Utilizing Ionic Liquids) Technology: The First Commercialized process with Ionic Liquids, *Kagaku Kogaku*, **2006**, *70*, 121-122.
- [5] C. Lorbeer, J. Cybinska, A.-V. Mudring, *J. Mat. Chem. C*, **2014**, *2*, 1862-1868. T. Alammar, H. Noei, Y. Wang, A.-V. Mudring, *Nanoscale*, **2013**, *5*, 8045-8055; P. Ghosh, S.-F. Tang, A.-V. Mudring, *J. Mater. Chem.* **2011**, *21*, 8640.
- [6] T. Alammar, Kit Chow, A.-V. Mudring, *New J. Chem.*, **2015**, *39*, 1339 – 1347; T. Alammar, H. Noei, Y. Wang, W. Grünert, A.-V. Mudring, *ACS Sustainable Chemistry and Engineering* **2015**, *3*, 42-54; T. Alammar, O. Shekhah, J. Wohlgemuth, A.-V. Mudring: *J. Mater. Chem.*, **2012**, *22*, 18252-18260. T. Alammar, A.-V. Mudring, *ChemSusChem*, **2011**, *12*, 1796-1804.
- [7] G. Wang, M. Valldor, B. Mallick, A.-V. Mudring, *J. Mat. Chem. C* **2014**, *2*, 7417-7427. G. Wang, M. Valldor, C. Lorbeer, A.-V. Mudring, *Eur. J. Inorg. Chem.*, **2012**, *18*, 3032-3038. G. Wang, A.-V. Mudring, *Crystals*, **2011**, *1*, 22-27.
- [8] M.J. Earle, S.P. Katadare, K.R. Seddon, *Org. Lett.* **2004**, *6*, 707-710; P. Pavez, D. Millán, C. Cocq, J. G. Santos, F. Nome, *New J. Chem.* **2015**, *39*, 1953-1959.
- [9] J. Fuller, R.T. Carlin, H.C. De Long, D. Haworth, *J. Chem. Soc., Chem. Commun.* **1994**, 299-300; J.D. Holbrey, W.M. Reichert, M. Nieuwenhuyzen, S. Johnston, K.R. Seddon, R.D. Rogers, *Chem. Commun.* **2003**, 1636-1637; A.S. Larsen, J.D. Holbrey, F.S. Tham, C.A. Reed, *J. Am. Chem. Soc.* **2000**, *122*, 7264-7272; P.A.Z. Suarez, J.E.L. Dullius, S. Einloft, R.F. DeSouza, J. Dupont, *Polyhedron* **1996**, *15*, 1217-1219; J.S. Wilkes, M.J. Zaworotko, *J. Chem. Soc. Chem. Commun.* **1992**, 965; S.A. Forsyth, J.M. Pringle, D.R. MacFarlane, *Austr. J. Chem.* **2004**, *57*, 113-119.
- [10] P.M. Dean, J. Turanjanin, M. Yoshizawa-Fujita, D. MacFarlane, J. Scott, *Cryst. Growth & Design* **2009**, *9*, 1137-1145.
- [11] J. Stoimenovski, D.R. MacFarlane, K. Bica, R.D. Rogers, *Pharm. Res.* **2010**, *27*, 521.

- [12] C. Warren, *Am. J. Med. Sci.* **1916**, *152*, 569-574.
- [13] H. Al-Humadi, S. Theocharis, I. Dontas, V. Stolakis, A. Zarros, A. Kyriakaki, R. Al-Saigh, C. Liapi, *Dig. Dis. Sci.* **2012**, *57*, 3168–3177.
- [14] Tammann, *Kristallisieren und Schmelzen*, J.A. Barth, Leipzig, 1903.
- [15] B. Mallick, A. Melten, M. Nieuwenhuyzen, R.-D. Rogers, A.-V. Mudring, *Inorg. Chem.*, **2012**, *51* (1), 193-200; A.S.R. Chesman, M. Yang, B. Mallick, T.M. Ross, I.A. Gass, G.B. Deacon, S.R. Batten, A.-V. Mudring, *Chem. Commun.*, **2012**, *48*, 124-126. D. Yaprak, E.T. Spielberg, T. Bäcker, M. Richter, B. Mallick, A. Klein, A.-V. Mudring, *Chem. Eur. J.* **2014**, *20*, 6482-6493; E.T. Spielberg, E. Edengeißer, B. Mallick, M. Havenith, A.-V. Mudring, *Chem. Eur. J.*, **2014**, *20*, 5338-5345; S.F. Tang, C. Lorbeer, X. Wang, P. Ghosh, A.-V. Mudring, *Inorg. Chem.* **2014**, *53*, 9027-99035.
- [16] A. R. Choudhury, N. Winterton, A. Steiner, A.I. Cooper, K.A. Johnson, *J. Am. Chem. Soc.* **2005**, *127*, 16792; A. R. Choudhury, N. Winterton, A. Steiner, A.I. Cooper, K.A. Johnson, *CrystEngComm* **2006**, *8*, 742; P. Nockemann, K. Binnemans, B. Thijs, T.N. Parac-Vogt, K. Merz, A.-V. Mudring, P.C. Menon, R.N. Rajesh, G.Cordoyiannis, J. Thoen, J. Leys, C. Glorieux, *J. Phys. Chem. B*, **2009**, *113*, 1429; T. Bäcker, O. Breunig, M. Valldor, K. Merz, V. Vasylyeva, A.-V. Mudring, *Cryst. Growth Des.*, **2011**, *11*, 2564-2571.
- [17] V.R. Thalladi, H.-C. Weiss, D. Bläser, R. Boese, A. Nangia, G.R. Desiraju, G. R. *J. Am. Chem. Soc.* **1998**, *120*, 8702-8710.
- [18] J. Fuller, R.T. Carlin, H.C. De Long, D. Haworth, *J. Chem. Soc., Chem. Commun.* **1994**, 299.
- [19] S. Saha, S. Hayashi, A. Kobayashi, H. Hamaguchi, *Chem. Lett.* **2003**, *32*, 740; M. Klapötke, P. Mayer, A. Schulz, J.J. Weigand, *J. Am. Chem. Soc.* **2005**, *127*, 2032; S. Schneider, T. Hawkins, M. Rosander, J. Mills, A. Brand, L. Hudgens, G. Warmoth, A. Vij, *Inorg. Chem.* **2008**, *47*, 3617.
- [20] W. Pei, X. Si, D. Ji, J. Ji, *Acta Cryst. E* **2008**, *64*, o721.
- [21] P.B. Hitchcock, R.J. Lewis, T. Welton, *Polyhedron* **1993**, *12*, 2039.
- [22] D. Zhao, Z. Fei, R. Scopelliti, P.J. Dyson, *Inorg. Chem.* **2004**, *43*, 2197.
- [23] K. Ganesan, Y. Alias, S.W. Ng, *Acta Cryst. C*, **2008**, *64*, o478.
- [24] A. Getsis, A.-V. Mudring, *Cryst. Res. Technol.* **2008**, *43*, 1187; A. Getsis, A.-V. Mudring, *Acta Cryst.* **2005**, *E61*, o2945.
- [25] J. Lachwa, I. Bento, M.T. Duarte, J.N.C Lopes, L.P.N. Rebelo, *Chem. Commun.* **2006**, 2445.
- [26] T. Kottke, D. Stalke, *J. Appl. Crystallogr.* **1993**, *26*, 615.
- [27] www.hamptonresearch.com

[28] A.-V. Mudring, A. Babai, S. Arenz, R. Giernoth, *Angew. Chem. Int. Ed.*, **2005**, *44*, 5485-5488.